Velocity distribution function and transport coefficients of electron swarms in gases. II. Moment equations and applications

K. F. Ness* and R. E. Robson
Physics Department, James Cook University of North Queensland, Townsville, Queensland, Australia 4811
(Received 27 January 1986)

A representation of the hierarchy of kinetic equations formulated earlier [Phys. Rev. A 33, 2068 (1986)] for reacting charged-particle swarms in gases is obtained in the Sonine polynomial basis. We specialize to electron swarms and compute transport and rate coefficients, distribution functions, and other quantities of physical interest for both model and realistic electron-molecule scattering cross sections, in a wide variety of cases.

I. INTRODUCTION

In the preceding paper[1] (referred to hereafter as I) we considered the more formal aspects of the kinetic theory of the reacting charged-particle swarms in gaseous media and derived a hierarchy of kinetic equations which must in general be solved numerically, e.g., by representing the functions as a series of orthogonal polynomials or by finite element techniques. We give a discussion of the former approach in the present paper and, as in Lin, Robson, and Mason,[2] specify the basis in terms of Sonine (generalized Laguerre) polynomials, well known in the kinetic theory of gases.[3] The problem then reduces to finding first the representation of Eqs. (I.28)—(I.31) in this basis and second the solution of these "moment" equations. Both processes are rather long and involved therefore we outline only the most important features in Sec. II. For a comprehensive discussion, the reader is referred to the thesis of Ness.[4] In Sec. III, we report on the results of computation of electron swarm transport coefficients, distribution functions, and other quantities of physical interest, for a wide variety of gases. We use model cross sections to elucidate physical phenomena where appropriate, but where realistic cross sections are known, these are incorporated in the calculations. Our results are in good agreement with both experiment and other theoretical predictions, where these are available.

II. MOMENT EQUATIONS

A. Hierarchy of equations and transport coefficients

The density gradient decomposition of the spherical harmonics coefficients is, to second order [cf. (I.13)],

$$f_m^{(l)}=\sum_{s=0}^{2}\sum_{\lambda=0}^{s} f(lm\mid s\lambda)G_m^{(s\lambda)}n\ , \tag{1}$$

where $f(lm\mid s\lambda)$ depends upon speed c, but not position or time. The meaning of the tensor operator $G^{(s\lambda)}$ is discussed in I Sec. II 2. We expand these quantities about a Maxwellian velocity distribution function at some arbitrary temperature T_b in terms of Sonine polynomials[3]

$$f(lm\mid s\lambda)=\bar{w}(\alpha,c)\sum_{\nu=0}^{\infty} F(\nu lm\mid s\lambda)R_{\nu l}(\alpha c)\ , \tag{2}$$

where

$$R_{\nu l}(c)\equiv N_{\nu l}(c/\sqrt{2})^l S_{l+1/2}^{(\nu)}(c^2/2)\ , \tag{3a}$$

$$\bar{w}(\alpha,c)\equiv(\alpha^2/2\pi)^{3/2}\exp(-\alpha^2c^2/2)\ , \tag{3b}$$

$$N_{\nu l}\equiv[2\pi^{3/2}\nu!/\Gamma(\nu+l+\tfrac{3}{2})]^{1/2}\ , \tag{3c}$$

$$\alpha\equiv(m/kT_b)^{1/2}\ . \tag{3d}$$

Representation (2) is to be compared with (I.4), with

$$\xi_{\nu l}(c)=n\bar{w}(\alpha,c)R_{\nu l}(\alpha c)\ .$$

The parameter T_b (and therefore α) is essentially unconstrained and is chosen ultimately in numerical calculations in such a way as to optimize convergence of our expansions. This single free-parameter basis set suffices for present purposes, i.e., for computation of electron swarm properties, but more elaborate representation are possible (and desirable) for other cases.[5,6]

The combined spherical-harmonic—Sonine-polynomial expansions amount to representation of the distribution function in terms of the well-known Burnett functions.[2–6] Equations (6)—(9) following are the corresponding representation of Boltzmann's equation (I.3), or simply "moment equations." Orthogonality of the Sonine polynomials[3] leads to the result

$$\int_0^\infty \bar{w}(\alpha,c)R_{\nu l}(\alpha c)R_{\nu' l}(\alpha c)c^2\,dc=\delta_{\nu'\nu}\ ,$$

and hence from (2),

$$F(\nu lm\mid s\lambda)=\int_0^\infty f(lm\mid s\lambda)R_{\nu l}(\alpha c)c^2\,dc\ . \tag{4}$$

It then follows from (I.14a), (I.14b), (I.37a), and (I.37b) that

$$F(\nu l-m\mid s\lambda)=F(\nu lm\mid s\lambda)\ , \tag{5a}$$

$$F(\nu lm\mid s\lambda)=0\ \text{ if }\ \mid m\mid>\min\{l,\lambda\}\ , \tag{5b}$$

$$F(000\mid s\lambda)=\delta_{s0}\delta_{\lambda 0}\ , \tag{5c}$$

the last equation representing the normalization condition.

If we multiply each of equations (I.28), (I.29), (I.30), and (I.31) by $R_{\nu l}(\alpha c)c^2$ and integrate over all speeds c, we obtain the following hierarchy of matrix equations for the quantities $F(\nu lm \mid s\lambda)$: For $s=\lambda=0$,

$$\sum_{\nu',l'}[M_{\nu l,\nu' l'}(0)+\omega(00)\delta_{\nu\nu'}\delta_{l'l}]F(\nu' l'0\mid 00)=0,\quad \nu,l=0,1,2,\ldots,\infty\ ; \tag{6}$$

for $s=\lambda=1$

$$\sum_{\nu',l'}[M_{\nu l,\nu' l'}(m)+\omega(00)\delta_{\nu\nu'}\delta_{l'l}]F(\nu' l'm\mid 11)$$
$$=-\omega(11)F(\nu l0\mid 00)\delta_{m0}-\frac{1}{\alpha}\sum_{\nu',l'}(\nu l||\alpha c^{[1]}||\nu' l')(1ml'0\mid lm)F(\nu' l'0\mid 00)\ ,\quad \nu,l=0,1,2,\ldots,\infty,\quad m=0,\pm1\ ; \tag{7}$$

for $s=2$, $\lambda=0$,

$$\sum_{\nu',l'}[M_{\nu l,\nu' l'}(0)+\omega(00)\delta_{\nu\nu'}\delta_{l'l}]F(\nu' l'0\mid 20)$$
$$=-\omega(20)F(\nu l0\mid 00)+\frac{1}{\sqrt{3}}\omega(11)F(\nu l0\mid 11)$$
$$-\frac{1}{\alpha}\sum_{\nu',l',m'}(\nu l||\alpha c^{[1]}||\nu' l')F(\nu' l'm'\mid 11)(1-m'l'm'\mid l0)\frac{(-1)^{1-m'}}{\sqrt{3}}\ ,\quad \nu,l=0,1,2,\ldots,\infty\ ; \tag{8}$$

for $s=2$, $\lambda=2$,

$$\sum_{\nu',l'}[M_{\nu l,\nu' l'}(m)+\omega(00)\delta_{\nu\nu'}\delta_{l'l}]F(\nu' l'm\mid 22)$$
$$=-\omega(22)F(\nu l0\mid 00)\delta_{m0}-(101m\mid 2m)\omega(11)F(\nu lm\mid 11)$$
$$-\frac{1}{\alpha}\sum_{\nu',l',m'}(\nu l||\alpha c^{[1]}||\nu' l')F(\nu' l'm'\mid 11)(1m-m'l'm'\mid lm)(1m-m'1m'\mid 2m)\ ,$$
$$\nu,l=0,1,2,\ldots,\infty,\quad m=0,\pm1,\pm2\ . \tag{9}$$

The matrix M is defined by

$$M_{\nu l,\nu' l'}(m)\equiv n_0 J^l_{\nu\nu'}\delta_{l'l}+i\alpha a(\nu l||K^{[1]}||\nu' l')(10l'm\mid lm)\ , \tag{10}$$

where, for a gas of neutral molecules of number density n_0,

$$J^l_{\nu\nu'}\equiv\frac{1}{n_0}\int_0^\infty R_{\nu l}(\alpha c)J^l[w(\alpha,c)R_{\nu' l}(\alpha c)]c^2\,dc \tag{11}$$

is the collision matrix [in Ref. 2, a related matrix, $a_{\nu\nu'}(l)=(N_{\nu' l}/N_{\nu l})J^l_{\nu\nu'}$ was used] and

$$(\nu l||\alpha c^{[1]}||\nu' l')\equiv\int_0^\infty R_{\nu l}(c)\langle l||c^{[1]}||l'\rangle\bar{w}(1,c)R_{\nu' l'}(c)c^2\,dc\ , \tag{12a}$$

$$(\nu l||K^{[1]}||\nu' l')\equiv\int_0^\infty R_{\nu l}(c)\langle l||\partial_c^{[1]}||l'\rangle\bar{w}(1,c)R_{\nu' l'}(c)c^2\,dc\ . \tag{12b}$$

It is useful at this stage to recall the quantities of physical interest. These are given by (I.27):

$$\alpha=-\omega(00) \tag{13a}$$

is the attachment loss rate,

$$W=i\omega(11) \tag{13b}$$

the drift velocity,

$$D_L=\frac{1}{\sqrt{3}}[\omega(20)-\sqrt{2}\omega(22)] \tag{13c}$$

the longitudinal diffusion coefficient, and

$$D_T=\frac{1}{\sqrt{3}}\left[\omega(20)+\frac{1}{\sqrt{2}}\omega(22)\right] \tag{13d}$$

the transverse diffusion coefficient. It is obvious then why we focus our attention on the $\omega(s\lambda)$ in the subsequent discussion.

Properties of the Wigner (Clebsch-Gordan) coefficients were given in I in Sec. II A 1. The operators J^l, $\langle l||c^{[1]}||l'\rangle$, and $\langle l||\partial_c^{[1]}||l'\rangle$ were defined in (I.18), (I.20), and (I.21), respectively. Equations (11) and (12) are effectively the representations of these operators in the Sonine polynomial basis. Explicit expressions can be found in the Appendix of Ref. 5 [(A43) and (A44)]. Summations in ν' and l' run over all allowed values, i.e., from 0 to ∞ in Eqs. (6)–(9).

Solution of (6) amounts to finding the eigenvalues and eigenfunctions of M. As explained in I in Sec. II B 3, the physics of the problem dictates which eigenvalue is to be selected from the spectrum. The matrix M is not Hermitian and, at the time of writing, very little is known about the general properties of this spectrum—one simply has to rely upon numerical estimations. The corresponding eigenfunctions are specified using the normalization condition (5c), viz., $F(000|00)=1$. The $\omega(00)$ and $F(\nu l0\mid 00)$ found from (6) are required to effect solution of higher-order members of the chain.

If we set $\nu=0=l$ in (6) and note that

$$(00||K^{[1]}||\nu'l')$$
$$=\sqrt{4\pi}\int_0^\infty \langle 0||\partial_c^{[1]}||l'\rangle \bar{w}(1,c)R_{\nu l'}(c)c^2\,dc$$
$$\equiv 0$$

by virtue of (I.38), then it follows that

$$\omega(00)=-n_0\sum_{\nu'=0}^{\infty} J^0_{0\nu}F(\nu'00\,|\,00)\,, \tag{14}$$

corresponding to (I.39). Only the reactive part of the collision matrix contributes, as explained in Sec. II B following. This is not always a particularly useful relationship, for one needs to have the solution to (6) in order to evaluate the right-hand side (rhs) and in that case, one would already know $\omega(00)$. However, if all terms in the summation for which $\nu'\geq 1$ are neglected it follows with the normalization condition that

$$\omega(00)\approx -n_0 J^0_{00}\,.$$

This approximation amounts to assuming that the distribution function is Maxwellian. Such a low order of truncation (effectively $\nu_{\max}=0$) is rarely adequate, however, and systematic solution of the doubly infinite matrix equation (6) by successive incrementation of $\nu_{\max}, l_{\max}$ until convergence is achieved is generally required.

On the other hand, setting $\nu=l=m=0$ in (7) leads to quite useful information:

$$\omega(11)=\frac{1}{\alpha}F(010\,|\,00)-n_0\sum_{\nu'=1}^{\infty} J^0_{0\nu}F(\nu'00\,|\,11)\,. \tag{15}$$

In deriving this we have used the fact that $(00||K^{[1]}||\nu'l')=0$, $(00||\alpha c^{[1]}||\nu'l')=\sqrt{3}\delta_{\nu 0}\delta_{l'1}$, and $(1010|00)=-1/\sqrt{3}$. This corresponds to (I.40). Substitution of (15) into (7) yields

$$\sum_{\nu',l}{}'[M_{\nu l,\nu'l'}(m)+\omega(00)\delta_{\nu'\nu}\delta_{l'l}-n_0J^0_{0\nu}F(\nu l0\,|\,00)\delta_{l'0}\delta_{m0}]F(\nu'l'm\,|\,11)$$
$$=-\frac{1}{\alpha}F(010\,|\,00)F(\nu l0\,|\,00)\delta_{m0}-\frac{1}{\alpha}\sum_{\nu',l'}(\nu l||\alpha c^{[1]}||\nu'l')(1ml'0\,|\,lm)F(\nu'l'0\,|\,00)\,,$$
$$\nu,l=0,1,2,\ldots,\infty,\quad m=0,\pm1\ \text{ but }\ (\nu,l,m)\neq(0,0,0)\,. \tag{16}$$

The prime on the summation in the left-hand side (lhs) indicates that there is no term for which $(\nu',l')=(0,0)$. Likewise, the $(\nu,l)=(0,0)$ member of (16) is identically zero on both sides, and need not be taken into consideration. Equations (16) constitute an infinite set of equations for $F(\nu lm\,|\,11)[(\nu,l,m)\neq(0,0,0)]$ which, when solved, yield $\omega(11)$ through Eq. (15). Notice that the $m=\pm1$ equations are essentially the same. Symmetry with respect to the sign of m has already been observed [see (5a)] and is a reflection of geometrical symmetry (specifically, invariance under rotations about the z axis) in configuration space.

Other members of the hierarchy are treated similarly. Thus we find

$$\omega(20)=-\frac{1}{\alpha\sqrt{3}}[F(010\,|\,11)+2F(011\,|\,11)]-n_0\sum_{\nu'=1}^{\infty}J^0_{0\nu}F(\nu'00\,|\,20)\,, \tag{17}$$

$$\sum_{\nu',l'}{}'[M_{\nu l,\nu'l'}(0)+\omega(00)\delta_{\nu'\nu}\delta_{l'l}-n_0J^0_{0\nu}F(\nu l0\,|\,00)\delta_{l'0}]F(\nu'l'0\,|\,20)$$
$$=\frac{1}{\alpha\sqrt{3}}F(\nu l0\,|\,00)[F(010\,|\,11)+2F(011\,|\,11)]+\frac{1}{\sqrt{3}}\omega(11)F(\nu l0\,|\,11)$$
$$-\frac{1}{\alpha\sqrt{3}}\sum_{\nu',l',m'}{}'(\nu l||\alpha c^{[1]}||\nu'l')(1-m'l'm'\,|\,l0)(-1)^{1-m'}F(\nu'l'm'\,|\,11)\,,$$
$$\nu,l=0,1,2,\ldots,\infty,\ \text{ but }\ (\nu,l)\neq(0,0)\,, \tag{18}$$

$$\omega(22)=\frac{1}{\alpha}\sqrt{2/3}[F(010\,|\,11)-F(011\,|\,11)]-n_0\sum_{\nu'=1}^{\infty}J^0_{0\nu}F(\nu'00\,|\,22)\,, \tag{19}$$

$$\sum_{\nu',l'}{}'[M_{\nu l,\nu'l'}(m)+\omega(00)\delta_{\nu'\nu}\delta_{l'l}-n_0J^0_{0\nu}F(\nu l0\,|\,00)\delta_{m0}\delta_{l'0}]F(\nu'l'm\,|\,22)$$
$$=\frac{1}{\alpha}\sqrt{2/3}\delta_{m0}F(\nu l0\,|\,00)[F(011\,|\,11)-F(010\,|\,11)]-(101m\,|\,2m)\omega(11)F(\nu lm\,|\,11)$$
$$-\frac{1}{\alpha}\sum_{\nu',l',m'}{}'(\nu l||\alpha c^{[1]}||\nu'l')(1m-m'l'm'\,|\,lm)(1m-m'1m'\,|\,2m)F(\nu'l'm'\,|\,11)\,. \tag{20}$$
$$\nu,l=0,1,2,\ldots,\infty,\quad m=0,\pm1,\pm2,\ \text{ but }\ (\nu,l,m)\neq(0,0,0)\,.$$

Equations (17) and (19) correspond to Eqs. (I.41) and (I.42), respectively. Note that only the $m=0$ member of the set (20) is required to find $\omega(22)$ and that symmetry exists with respect to the sign of m otherwise.

The procedure is then as follows.

(i) Solve the eigenvalue problem (6) to obtain $\omega(00)$ and $F(\nu l0\,|\,00)$.

(ii) Solve the inhomogeneous equations (16) for $m=0,1$, using the result of step (i), to obtain $F(\nu lm\,|\,11)$. Obtain $\omega(11)$ from (15).

(iii) With these results, solve (18) for $F(\nu l0\,|\,20)$ and (20) for $F(\nu l0\,|\,22)$ and find $\omega(20)$ and $\omega(22)$ from (17) and (19), respectively.

(iv) Obtain transport and rate coefficients from Eqs. (13).

It can be seen that there are *five* sets of equations to be solved for the *four* quantities of physical interest.

B. Interactions and collision matrix

The foregoing equations are all quite general. The only assumption we have made is that the interactions between swarm particles and neutral molecules operate through central forces, with the result that the collision matrix $J^l_{\nu\nu'}$ is diagonal in l and m indices and independent of the latter. [See (I.18).] Our analysis is therefore, in principle at least, applicable to ions as well as electrons; specialization to the latter case only comes about when certain approximations are made regarding the smallness of the swarm particle—neutral molecule mass ratio m/m_0, for computational purposes. The following discussion on collisional processes could just as easily have been framed in terms of ion-molecule interactions and reactions as for electron-molecule scattering phenomena, but we choose to refer to "electrons" from this point on, for the sake of definiteness and with future applications in mind.

1. Elastic and inelastic (particle-conserving) processes

We denote by $\sigma(jk;g\Omega)$ the differential cross section for scattering of an electron of mass m, velocity $\mathbf{c}$ from a neutral molecule of mass m_0, velocity $\mathbf{c}_0$, which is initially in an internal state characterized by quantum number (or set of quantum numbers) j. The corresponding post collision velocities are $\mathbf{c}'$ and $\mathbf{c}_0'$, respectively, and the new internal state of the molecule is designated by k. Relative velocities before and after a collision, $\mathbf{g}$ and $\mathbf{g}'$, respectively, are related through the energy conservation requirement

$$\tfrac{1}{2}\mu g^2+\varepsilon_j=\tfrac{1}{2}\mu(g')^2+\varepsilon_k\ , \tag{21}$$

where $\mu\equiv mm_0/(m+m_0)$ is the reduced mass and ε_j is the internal energy of a molecule in state j. It is assumed that the neutral gas is in equilibrium at temperature T_0, so that the number density of molecules in state j is given by

$$n_{0j}=n_0\omega_j Z_0^{-1}\exp(-\varepsilon_j/kT_0)\ , \tag{22}$$

where ω_j is the degeneracy of energy level ε_j and

$$Z_0\equiv\sum_j \omega_j e^{-\varepsilon_j/kT_0}\ .$$

An elastic collision occurs if $j=k$. Superelastic processes are those for which $\varepsilon_k<\varepsilon_j$, i.e., the molecule makes a transition to a lower energy state upon electron impact. These are absent for a "cold gas" ($T_0=0$), an assumption made either explicitly or implicitly in some works.

As in Ref. 2, we assume that the Wang-Chang *et al.*[7] generalization of the Boltzmann collision operator describes these processes, and write for the particle-conserving collision operator

$${}^cJ(f)=\sum_{j,k}\int\int[f(\mathbf{c})f_{0j}(\mathbf{c}_0)-f(\mathbf{c}')f_{0k}(\mathbf{c}_0')]g\sigma(jk;g\Omega)d\Omega\,d\mathbf{c}_0\ , \tag{23}$$

where the neutral molecule distribution function is

$$f_{0j}(\mathbf{c}_0)=n_{0j}\bar{w}(\alpha_0,c_0) \tag{24}$$

and

$$\alpha_0\equiv(m_0/kT_0)^{1/2}\ .$$

As explained elsewhere,[2,8] the matrix elements corresponding to (23) can be written as

$${}^cJ^{l_1}_{\nu_1\nu_2}=\sum_{\nu,l,\bar{\nu}}\langle l_1\nu_1\nu_2\,|\,l\nu\bar{\nu}\rangle\,{}^cU^l_{\nu\bar{\nu}}\ , \tag{25}$$

where $\langle l_1\nu_1\nu_2\,|\,l\nu\bar{\nu}\rangle$ are coefficients which involve mass and temperature ratios and

$${}^cU^l_{\nu\bar{\nu}}\equiv\sum_{j,k}\frac{n_{0j}}{n_0}\,{}^cV^l_{\nu\bar{\nu}}(jk)\ . \tag{26}$$

The summation in (26) is over all possible quantum numbers j,k consistent with whatever selection rules are applicable for the transition $j\to k$. The interaction integrals

$${}^cV^l_{\nu\bar{\nu}}(jk)=\int_0^\infty\bar{w}(\gamma,g)R_{\bar{\nu}l}(\gamma g)[\sigma_0(jk;g)R_{\nu l}(\gamma g)-\sigma_l(jk;g)R_{\nu l}(\gamma g')]g^3\,dg \tag{27}$$

are by now well established in kinetic theory.[8,9] In (27), we have

$$\gamma=(\mu/kT_b)^{1/2}$$

and the partial cross sections

$$\sigma_l(jk;g)\equiv\int P_l(\cos\chi)\sigma(jk;g\Omega)d\Omega\ . \tag{28}$$

The coefficient $\langle 00\nu_2\,|\,l\nu\bar{\nu}\rangle$ vanishes unless $l=\nu=0$.[8] Equation (27) shows that ${}^cV^0_{0\bar{\nu}}(jk)\equiv 0$ and hence by (25) and (26) we have

$${}^cJ^0_{0\nu_2}\equiv 0\ , \tag{29}$$

i.e., the first row of the particle-conserving collision matrix vanishes.

2. Attachment

A review of analyses of attachment processes has been given by Tagashira.[10] (See also the treatise of Huxley and Crompton.[11]) The attachment rate[12] α is given by (13a) or equivalently by (I.53a). Phenomena such as attachment "cooling" and "heating" are by now well understood.[13] We assume an attachment collision operator

$$ {}^{A}J(f)=\left[\sum_{j}\int f_{0j}(\mathbf{c}_0)g\sigma_A(j;g)d\mathbf{c}_0\right]f(\mathbf{c}) , \tag{30}$$

where $\sigma_A(j;g)$ is the total cross section for attachment of an electron to a neutral molecule in state j. We do not find it necessary to assume that the gas is cold for purposes of analyzing this process.

Using the same Talmi-transformation methods[8,9] as employed in deriving (25), we find that the collision matrix corresponding to (30) is

$$ {}^{A}J^{l_1}_{\nu_1\nu_2}=\sum_{l,\nu,\bar{\nu}}\langle l_1\nu_1\nu_2\,|\,l,\nu\bar{\nu}\rangle\,{}^{A}U^{l}_{\nu\bar{\nu}} , \tag{31}$$

where

$$ {}^{A}U^{l}_{\nu\bar{\nu}}\equiv\sum_{j}n_{0j}/n_0\,{}^{A}V^{l}_{\nu\bar{\nu}}(j) , \tag{32}$$

$$ {}^{A}V^{l}_{\nu\bar{\nu}}(j)\equiv\int_0^\infty\bar{w}(\gamma,g)R_{\bar{\nu}l}(\gamma g)\sigma_A(j;g)R_{\nu l}(\gamma g)g^3\,dg . \tag{33}$$

Unlike the conservative interaction integrals (27), the corresponding attachment integrals (33) have no term arising from restitutional collisions. It is therefore clear that ${}^{A}V^{0}_{0\bar{\nu}}(j)$ is nonzero and hence

$$ {}^{A}J^{0}_{0\nu_2}\neq 0 , \tag{34}$$

in contrast to (29).

3. Ionization by electron impact

A detailed discussion of the ionization process, together with a review of previous analyses, can be found in Ref. 4. The theory of Sec. II A preceding applies also to ionization phenomena, with α replaced by $-\alpha$ in Eq. (13a).[14]

The dynamics of an ionizing collision are complicated, there being both a scattered and an ejected electron emerging after a collision, which, together with the gas molecule, comprises a three-body problem. As a first approximation, we can assume the molecule to be infinitely heavy and partition energy and momentum entirely between the electrons. (This is equivalent to taking only terms to zero order in m/m_0 in the expansion of the collision operator.)

With the above assumption, and considering only the one ionization process for simplicity, the appropriate ionization collision operator is[4]

$$ {}^{I}J(f)=n_0c\sigma_I(c)f(\mathbf{c}) -2n_0\int c'\sigma_I(c')B(\mathbf{c},\mathbf{c}')f(\mathbf{c}')d\mathbf{c}' , \tag{35}$$

where σ_I is the total ionization cross section and $B(\mathbf{c},\mathbf{c}')$ is a probability density that divides the available momentum after ionization between the two electrons. That is to say, $B(\mathbf{c},\mathbf{c}')d\mathbf{c}$ is the probability of one of the two electrons after ionization having a velocity between $\mathbf{c}$ and $\mathbf{c}+d\mathbf{c}$, given that the incident electron has velocity $\mathbf{c}'$. The factor of 2 in front of the second term on the rhs of (35) arises because after each ionization collision there are two indistinguishable electrons. If there is more than one ionization process, then the rhs of (35) will involve a summation over all ionization channels. The quantity $2B(\mathbf{c},\mathbf{c}')\sigma_I(c')$ may be thought of as a "differential" ionization cross section. For central force scattering,

$$ B(\mathbf{c},\mathbf{c}')=B(c,c',\hat{\mathbf{c}}\cdot\hat{\mathbf{c}}') , \tag{36}$$

where

$$ \hat{\mathbf{c}}\cdot\hat{\mathbf{c}}'=\cos\chi , \tag{37}$$

χ being the angle between $\mathbf{c}$ and $\mathbf{c}'$.

The ionization collision matrix in the Burnett function basis corresponding to (35) can be written in the form[4]

$$ {}^{I}J^{l_1}_{\nu_1\nu_2}={}^{I}\hat{V}^{l_1}_{\nu_1\nu_2}-2\,{}^{I}\tilde{V}^{l_1}_{\nu_1\nu_2} , \tag{38}$$

where

$$ {}^{I}\hat{V}^{l_1}_{\nu_1\nu_2}=\int_0^\infty\bar{w}(\alpha,c)R_{\nu_1l_1}(\alpha c)\sigma_I(c)R_{\nu_2l_1}(\alpha c)c^3\,dc , \tag{39a}$$

$$ {}^{I}\tilde{V}^{l_1}_{\nu_1\nu_2}=\int_0^\infty\int_0^\infty\bar{w}(\alpha,c')R_{\nu_1l_1}(\alpha c)\sigma_I(c')B_{l_1}(c,c') \times R_{\nu_2l_1}(\alpha c')(c')^3c^2\,dc'\,dc , \tag{39b}$$

$$ B_l(c,c')=2\pi\int_{-1}^{1}B(\mathbf{c},\mathbf{c}')P_l(\cos\chi)d(\cos\chi) . \tag{40}$$

The quantity $2B_l(c,c')\sigma_I(c')$ may be viewed as a partial ionization cross section. For isotropic scattering $B_l(c,c')=0$ for $l\geq 1$. Again as in (34) we have

$$ {}^{I}J^{0}_{0\nu_2}\neq 0 . \tag{41}$$

The complete collision matrix is then

$$ J^{l_1}_{\nu_1\nu_2}={}^{C}J^{l_1}_{\nu_1\nu_2}+{}^{A}J^{l_1}_{\nu_1\nu_2}+{}^{I}J^{l_1}_{\nu_1\nu_2} =\sum_{l,\nu,\bar{\nu}}\langle l_1\nu_1\nu_2\,|\,l\nu\bar{\nu}\rangle({}^{C}U^{l}_{\nu\bar{\nu}}+{}^{A}U^{l}_{\nu\bar{\nu}}) +{}^{I}\hat{V}^{l_1}_{\nu_1\nu_2}-2\,{}^{I}\tilde{V}^{l_1}_{\nu_1\nu_2} , \tag{42}$$

as follows from (25), (31), and (38).

C. Distribution function and mean energy

By Eq. (2) and (I.46a), (I.46b), and (I.46c) we have

$$ F_l(c)=i^l\left[\frac{2l+1}{4\pi}\right]^{1/2}\bar{w}(\alpha,c) \times\sum_{\nu=0}^{\infty}F(\nu l0\,|\,00)R_{\nu l}(\alpha c),\quad l\geq 0 \tag{43a}$$

$$ F^{(L)}_l(c)=i^l\left[\frac{2l+1}{4\pi}\right]^{1/2}\bar{w}(\alpha,c) \times\sum_{\nu=0}^{\infty}F(\nu l0\,|\,11)R_{\nu l}(\alpha c),\quad l\geq 0 \tag{43b}$$

$$F_l^{(T)}(c)=i^{l+1}\left[\frac{2l+1}{2\pi l(l+1)}\right]^{1/2}\bar{w}(\alpha,c)$$
$$\times\sum_{\nu=0}^{\infty}F(\nu l\,1\,|\,11)R_{\nu l}(\alpha c),\quad l\geq 1 \tag{43c}$$

and by (I.54), to first order in ∇n, the velocity distribution function is

$$f(\mathbf{r},\mathbf{c},t)=n(\mathbf{r},t)f^{(0)}(c,\theta)-f^{(L)}(c,\theta)\partial_z n\ ,$$
$$-f^{(T)}(c,\theta)(\cos\phi\,\partial_x n+\sin\phi\,\partial_y n)\ , \tag{44}$$

where

$$f^{(0)}(c,\theta)=\sum_{l=0}^{\infty}F_l(c)P_l(\cos\theta)\ , \tag{45a}$$

$$f^{(L)}(c,\theta)=\sum_{l=0}^{\infty}F_l^{(L)}(c)P_l(\cos\theta)\ , \tag{45b}$$

$$f^{(T)}(c,\theta)=\sum_{l=1}^{\infty}F_l^{(T)}(c)P_l^1(\theta)\ , \tag{45c}$$

and θ is the angle between $\mathbf{c}$ and the z axis.

Clearly then, knowledge of the "moments," as obtained from solution of the hierarchy of equations in Sec. II A preceding, furnishes the distribution of velocities. [Equations (43), (44), and (45) can be extended in an obvious way to include quantities of second order in density gradient.] Summations over ν and l are to be understood as being truncated at upper limits of $\nu_{\max}$ and $l_{\max}$, respectively, when it comes to practical computation.

Another quantity of physical interest, though not usually directly measured in experiment, is the mean energy per particle, defined by

$$\bar{\varepsilon}=\langle\tfrac{1}{2}mc^2\rangle=\frac{\int d\mathbf{r}\int d\mathbf{c}\,\tfrac{1}{2}mc^2 f(\mathbf{r},\mathbf{c},t)}{\int d\mathbf{r}\int d\mathbf{c}\,f(\mathbf{r},\mathbf{c},t)}\ , \tag{46}$$

where the integral over $\mathbf{r}$ runs over all space. Inserting the hydrodynamic expansion (44) for f then yields

$$\bar{\varepsilon}=\frac{\int d\mathbf{c}\,\tfrac{1}{2}mc^2 f^{(0)}(c,\theta)}{\int d\mathbf{c}\,f^{(0)}(c,\theta)}\ , \tag{47}$$

where it has been assumed that density vanishes at the boundaries. Equation (47) indicates that $\bar{\varepsilon}$ can also be regarded as the mean energy of a spatially homogeneous swarm characterized by the velocity distribution function $f^{(0)}$. One next substitutes (45a) for $f^{(0)}$ and carries out the integration over angles. If one then makes use of the normalization condition together with Eq. (4) with $\nu=1$, $l=m=s=\lambda=0$, and the fact that

$$R_{10}(\alpha c)=\left[\frac{8\pi}{3}\right]^{1/2}\left[\frac{3}{2}-\frac{\tfrac{1}{2}mc^2}{kT_b}\right]\ ,$$

then it can be shown that (47) yields

$$\bar{\varepsilon}=\tfrac{3}{2}kT_b[1-\tfrac{2}{3}F(100\,|\,00)]\ . \tag{48}$$

One can similarly define random energies $\frac{1}{2}kT_{||},\frac{1}{2}kT_{\perp}$ associated with motion parallel and perpendicular to the applied field $\mathbf{E}$ (i.e., the z axis) by

$$\tfrac{1}{2}kT_{||}=\tfrac{1}{2}m\langle(c_z-\langle c_z\rangle)^2\rangle\ , \tag{49a}$$

and

$$\tfrac{1}{2}kT_{\perp}=\tfrac{1}{2}m\langle c_x^2\rangle=\tfrac{1}{2}m\langle c_y^2\rangle\ , \tag{49b}$$

respectively. Like $\bar{\varepsilon}$, these can be expressed entirely in terms of a spatially homogeneous distribution function, and further algebra leads to the results[4]

$$T_{||}=T_b[1-\sqrt{2/3}F(100\,|\,00)$$
$$-2\sqrt{3}F(020\,|\,00)+F(010\,|\,00)^2]\ , \tag{50a}$$

$$T_{\perp}=T_b[1-\sqrt{2/3}F(100\,|\,00)-(1/\sqrt{3})F(020\,|\,00)]\ . \tag{50b}$$

The deviation of the ratio $T_{||}/T_{\perp}$ from unity is a useful measure of the degree of anisotropy in velocity space. The electron "temperature" is given by

$$T=\tfrac{1}{3}(T_{||}+2T_{\perp})\ . \tag{51}$$

It is clear the transport coefficients, distribution functions, and in fact, any quantity of physical interest can be determined from the "moments," $F(\nu lm\,|\,s\lambda)$, which are in turn determined completely by the hierarchy of equations in Sec. II A preceding.

D. Numerical calculations

In Sec. III following we present results of the calculation of properties of electron swarms based upon the foregoing equations. Although details of the numerical work are obviously important, we have opted in this paper to make only a few general observations. Separate publication of details of the numerical method is planned, based upon the thesis of Ness.[4] Our observations are as follows.

(i) Each of the five equations in our hierarchy is doubly infinite, with truncation in both spherical-harmonic and Sonine-polynomial indices required for practical purposes. That is, we set $l\leq l_{\max}$ and $\nu\leq\nu_{\max}$ and increment $l_{\max}$ and $\nu_{\max}$ independently until some convergence criterion is met. Generally speaking, large deviations from spherical symmetry in velocity space lead to large $l_{\max}$, while large $\nu_{\max}$ results from significant departures of speed distributions from a Maxwellian at temperature T_b.

(ii) The matrix $M_{\nu l,\nu l'}$ defined by (10) has a tridiagonal block structure ($l'=l,l\pm1$) and computing time can be significantly reduced as compared with the original program of Lin *et al.*,[2] if one takes advantage of this. The efficiency may be increased in this way by one to two orders of magnitude for larger values of $l_{\max}$.

(iii) Accurate computation of interaction integrals $V^l_{\nu\bar{\nu}}$, from which the collision matrix is formed through (42), is essential, otherwise errors can propagate and influence convergence of results. It has been found that the Gauss-Laguerre quadrature originally used by Lin *et al.* is adequate for most purposes, but fails for computation of $V^l_{\nu\bar{\nu}}$ when cross sections vary rapidly with energy at higher energies. Then one is better off using standard Newton-Cotes routines. A detailed discussion of these aspects can be found in Refs. 4 and 8.

(iv) Our expressions can be cast into a form more suit-

able for numerical work by transformations of the type indicated in I in Sec. III, and appropriate dimensionless groups identified. These details can be found in Ref. 4.

III. RESULTS AND DISCUSSION FOR ELECTRON SWARMS

To begin with, in Sec. III A only conservative collisions are treated, both model and real gases being considered. In Sec. III B the theory is applied to electron attachment and ionization. Through the use of models the effect of three-body electron attachment on the transport characteristics is considered in some detail. In both Secs. III A and III B all scattering is assumed isotropic unless otherwise stated and for the model inelastic collisions considered, the energy lost by the electron is equal to the threshold energy for the process, unless otherwise indicated. Finally, in Sec. III C, a summary of the work covered is given.

A. Conservative interactions

1. Reid's ramp model

In order to test the present theory to see how it compares with the work of others, we first consider Reid's inelastic ramp model. Reid[15] used a number of constant and ramp model inelastic cross sections in his Monte Carlo investigation of the validity of the two-term approximation for electrons swarms. The details of the model used here are as follows:

$$\sigma_{\rm el}=6.0\ \text{Å}^2 \ \text{(elastic cross section)},$$
$$\sigma_{\rm inel}=\begin{cases}10(\varepsilon-0.2)\ \text{Å}^2, & \varepsilon\geq 0.2\ \text{eV} \ \text{(inelastic cross section)}\\ 0, & \varepsilon<0.2\ \text{eV}\end{cases} \tag{52}$$
$$m_0=4\ \text{amu},\quad T_0=0\ .$$

This particular model has been investigated by many workers.[15–21] Using the present moment method the transport coefficients for model (52) have been calculated at $E/n_0=1$, 12, and 24 Td. The results are set out in Table I where they are compared with the cubic spline method of Pitchford *et al.*[16,17] (POR), the relaxation method of MacMahon[18,19] (McM), the finite element method (FEM), and path differential method (PDM) of Segur *et al.*,[20] and the Monte Carlo results of Reid,[15] Braglia *et al.*[21] (Brag), Skullerud[20] (Skul), and Penetrante

TABLE I. Comparison of transport coefficients for ramp inelastic model (52) calculated using moment (M) with those of Pitchford *et al.* (Refs. 16 and 17) (POR) MacMachon (Ref. 18) (McM), Segur *et al.* (Ref. 20) (FEM) and (PDM), Reid (Ref. 15), Braglia *et al.* (Ref. 21) (Brag), Skullerud (Ref. 20) (Skul), and Penetrante *et al.* (Ref. 17) (Penet). The numbers in parentheses give the error in the last significant figure.

E/N_0 (Td)	Method	W (10^4 m s^{-1})	n_0D_T (10^{24} m^{-1}s^{-1})	n_0D_L (10^{24} m^{-1}s^{-1})	$\bar{\varepsilon}$ (eV)
1	M (6 term)	1.272	0.9751	0.7591	0.1015
	POR (6 term)	1.272	0.9749		
	McM (6 term)	1.272			0.1015
	FEM	1.271	0.9749	0.7594	0.1015
	PDM	1.270	0.9735	0.7623	0.1018
	Reid (MC)	1.255(13)			0.1013(10)
	Brag (MC)	1.272(6)	0.975(10)		0.1014(5)
12	M (6 term)	6.839	1.135	0.5688	0.2689
	POR (6 term)	6.838	1.134	0.57	0.269
	McM (6 term)	6.84			0.269
	FEM	6.832	1.135	0.569	0.2689
	PDM	6.832	1.131	0.569	0.269
	Reid (MC)	6.87(7)			
	Brag (MC)	6.84(3)	1.136(10)		0.269(1)
	Penet (MC)	6.86(2)	1.16(4)	0.58(3)	0.270(1)
24	M (6 term)	8.886	1.134	0.4609	0.4079
	POR (6 term)	8.885	1.132	0.46	0.408
	McM (6 term)	8.89	1.133	0.460	0.408
	FEM	8.881	1.134	0.463	0.4074
	PDM	8.874	1.131	0.4613	0.4083
	Reid (MC)	8.89(9)	1.145(23)		0.408(2)
	Brag (MC)	8.88(4)	1.134(10)	0.473(5)	0.408(2)
	Skul (MC)	8.869	1.130	0.465	0.4074
	Penet (MC)	8.89(2)	1.16(4)	0.48(2)	0.409(1)

TABLE II. Convergence of the transport coefficients in the l index for ramp inelastic model at $E/n_0=12$ Td. The number in square brackets is the corresponding result of Pitchford *et al.* (Ref. 16) taken from Table I of Ref. 16.

l_{max}	W (10^4 m s^{-1})	n_0D_T (10^{24} m^{-1}s^{-1})	n_0D_L (10^{24} m^{-1}s^{-1})	$\bar{\varepsilon}$ (eV)
1	7.029[7.029]	1.369[1.369]	0.5066	0.2736
2	6.821	1.111	0.5739	0.2689
3	6.841[6.841]	1.137[1.110]	0.5684	0.2689
4	6.837	1.136	0.5690	0.2690
5	6.839[6.838]	1.135[1.134]	0.5688	0.2689
6	6.838	1.135	0.5689	0.2689
7	6.838[6.839]	1.135[1.134]	0.5688	0.2689

et al.[17] (Penet). The Monte Carlo calculations of Skullerud and the corrected result of Reid are from Table I of Ref. 20, while the D_L and $\bar{\varepsilon}$ calculation of Pitchford's cubic spline method are from Table I of Ref. 17.

In the present work, the error in numbers quoted for the moment method is not greater than ± 1 in the last significant figure shown, unless otherwise indicated. For a given l truncation this error is estimated from the convergence of the transport coefficients in the ν index and also from the variation in the converged values of the transport coefficients for different choices of T_b. Apart from the Monte Carlo results of Reid,[15] Braglia *et al.*[21] and Penetrante *et al.*[17] and the W and n_0D_T values of Pitchford *et al.*[16] the accuracy of the results of the other workers shown in Table I is not known. For the Monte Carlo work the number in parentheses in Table I gives the error in the last significant figure, and follows from the percentage error quoted in the appropriate reference. For POR[16] W has converged to 0.1% and D_T to 1%.

From a comparison of the moment method results with the others in Table I, it is evident that the agreement is consistent for all values of E/n_0 and for all transport coefficients. For W and D_T the results of POR are in good agreement with the present results and their D_L values for 12 and 24 Td agree to the two significant figures they give. The W and $\bar{\varepsilon}$ values of McM agree with our calculation to the number of significant figures shown by him. In the case of D_T and D_L for $E/n_0=24$ Td his results compare well with the present ones. For 1 and 12 Td no D_T or D_L values were given by MacMahon and it is not clear if difficulties were experienced in determining these numbers or whether no attempt was made to calculate them. Of the two methods considered by Segur *et al.*[20] their FEM results compare more favorably with ours. In concluding their work, Segur *et al.* state that of the two methods they consider "FEM is the most accurate and the most powerful."[20] The present work appears to confirm this. Apart from Reid's W result for 1 Td the Monte Carlo results agree with the moment results to within the specified error. (We assume that the accuracy of Skullerud's work is of the same order as the other Monte Carlo results.)

In Table II the variation of the transport coefficients with the truncation in the l index is shown for $E/n_0=12$ Td. Clearly the $l=1$ (two-term) approximation is inadequate. Included in Table II are the W and D_T values of Pitchford *et al.*[16] (the numbers in square brackets). We see that, apart from the D_T value for $l=3$, the convergence in the l index is almost identical. Comparing the moment method $l=2$ result for D_T with the POR result for $l=3$ we suspect that Pitchford *et al.* mistakenly gave their $l=2$ result instead of the one for $l=3$.

To complete the present investigation of Reid's ramp model, equations (43a), (43b), and (43c) have been used to calculate velocity distribution functions at $E/n_0=12$ Td. The functions F_0 and $n_0F_0^{(L)}$ are plotted in Fig. 1, while the functions F_1, $n_0F_1^{(L)}$, and $n_0F_1^{(T)}$ are shown in Fig. 2. These plots are in excellent agreement with those of Penetrante *et al.*[17] They, however, do not calculate the function $F_1^{(T)}$. A polar plot of the function $f^{(0)}(\varepsilon,\theta)$, showing contours of constant $f^{(0)}$, is given in Fig. 3, where it is compared with the corresponding function obtained for the hard-sphere model

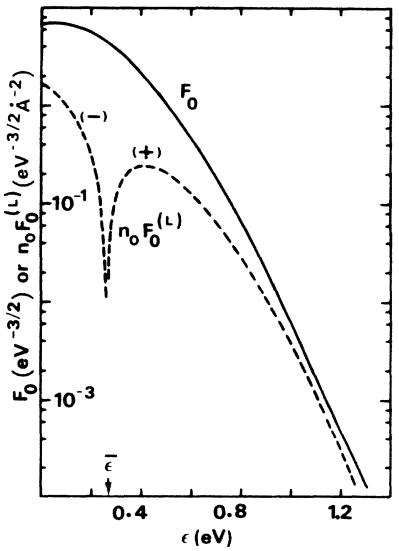

FIG. 1. Distribution functions $F_0(\varepsilon)$ and $n_0F_0^{(L)}(\varepsilon)$ for Reid's ramp model (52) at $E/n_0=12$ Td. For normalization purposes, these quantities differ from the functions defined in (43) by the factor $2\pi(2e/m)^{3/2}$.

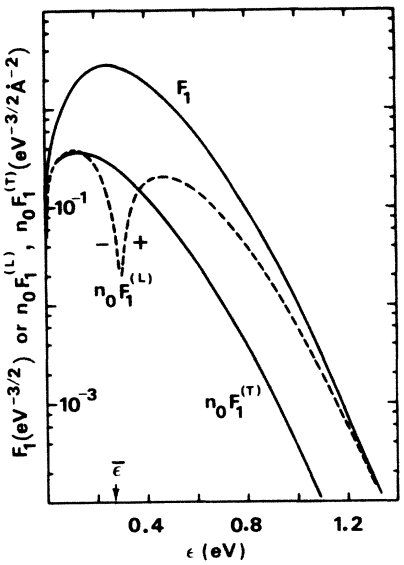

FIG. 2. Distribution functions $F_1(\varepsilon)$, $n_0F_1^{(L)}(\varepsilon)$, and $n_0F_i^{(T)}(\varepsilon)$ for Reid's ramp model (52) for $E/n_0=12$ Td. Normalization as in Fig. 1.

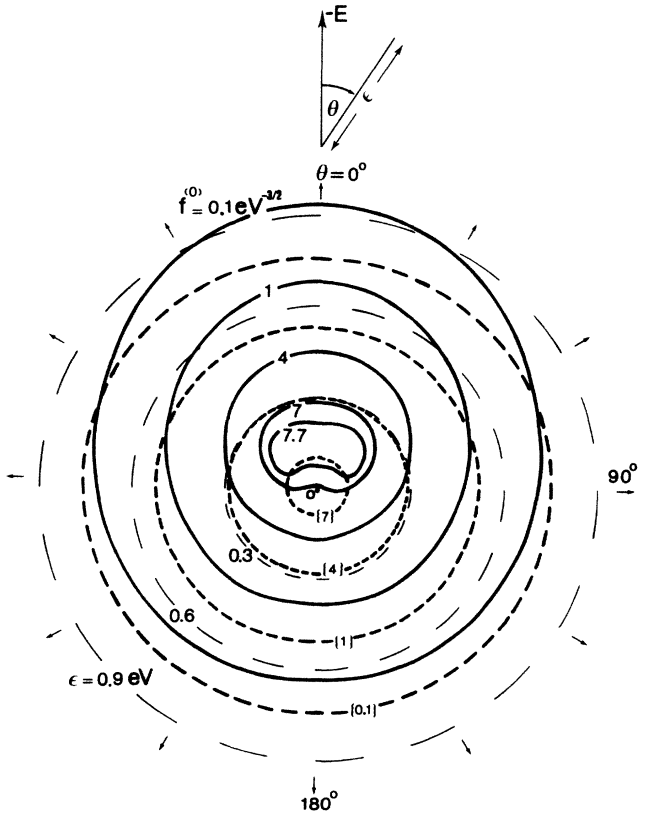

FIG. 3. Contours of constant $f^{(0)}(\varepsilon,\theta)$ in units of $(\text{eV})^{-3/2}$ for Reid's ramp model (52) (solid lines) at $E/n_0=12$ Td and the hard sphere model (53) (thick dashed lines, values of $f^{(0)}$ shown in curly brackets) at $E/n_0=0.44$ Td. The angle θ is marked in increments of 30° from 0° to 180° and three energy contours, 0.3, 0.6, and 0.9 eV are shown (thin dashed lines). This quantity differs from the distribution function (45a) through the factor $2\pi(2e/m)^{3/2}$.

$$\sigma_{el}=6\ \text{Å}^2\,,\qquad m_0=4\ \text{amu},\quad T_0=0\,, \tag{53}$$

[i.e., the elastic cross section only of model (52)] at $E/n_0=0.44$ Td. This value of E/n_0 was chosen because at this value the mean energy is 0.267 eV, which is very near the mean energy for model (52) at $E/n_0=12$ Td. For the hard-sphere model the $l=1$ approximation is sufficient, and this fact is reflected by the almost spherical symmetry ($T_{||}/T_\perp=1.0003$) in Fig. 3. On the other hand, for the ramp inelastic model Table II shows that the $l=1$ approximation is inadequate and this is reflected in Fig. 3 by the asymmetry ($T_{||}/T_\perp=1.084$) in velocity space.

The plot of $f^{(0)}(\varepsilon,\theta)$ may be thought of as a slice through the x-z or y-z plane in velocity space. For the $f^{(0)}=0.1$, 1, and 4 $(\text{ev})^{-3/2}$ contours of Reid's model we see that the anisotropy is such that for a given value of $f^{(0)}$ the most energetic electrons move in the $\theta=0$ direction. Intuitively we expect this, since this is the direction of the applied force acting on the electrons. For the 7 and 7.7 contours however, we observe a flattening out and the formation of a depression in the $\theta=0$ direction, with the most energetic electrons now tending to move in the $\theta\sim30°$ direction. For $f^{(0)}\sim7$ the energy of the electrons is of the order of 0.2 eV. This is the threshold energy for the single inelastic process, and so electrons with $\varepsilon<0.2$ eV undergo only elastic collisions, losing very little of their energy, while electrons with energy a little greater than 0.2 eV may also undergo inelastic collisions, losing almost all their energy. Thus for the electrons of energy ~0.2 eV the more energetic ones tend to move in the $\theta\sim0$ direction and may undergo inelastic collisions and be scattered well out of the energy range, while the less energetic electrons moving in other directions undergo elastic collision only and do not scatter far in energy space. Hence the formation of the depression in the $\theta\sim0$ direction in the contours of $f^{(0)}$ where $\varepsilon\sim0.2$ eV. Also note that for these values of $f^{(0)}$ no electrons move in the direction opposite to the force, i.e., $\theta=180°$.

2. *Methane*

Using the recently derived cross sections of Haddad,[22] an investigation of electron transport in methane for E/n_0 in the range 0.01 to 15 Td has been carried out. The cross sections, assumed isotropic,[23] are read in from a data file and linear interpolation is used to find the value at the quadrature points in the calculation of the interactions integrals. In Figs. 4 and 5 the coefficients W, $\bar{\varepsilon}$, D_T/μ, and D_L/μ have been plotted as functions of E/n_0. In the case of W and D_T/μ the experimental points of Haddad[22] are also shown. Over the range of E/n_0 considered we see that there is excellent agreement between experiment and theory. This agreement is not surprising however, since the present theory was used in the data analysis to obtain the cross sections.[22] From the plot of W it is seen that electrons in CH_4 exhibit negative differential conductivity, i.e., over a range of E/n_0 values the drift velocity decreases as the field is increased. Conditions leading to this phenomena have been discussed by Robson[24] and Petrovic *et al.*[25]

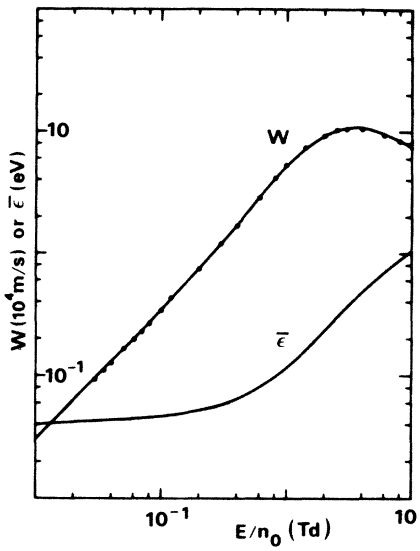

FIG. 4. Drift velocity and mean energy as a function of E/n_0 for electrons in CH_4 (solid lines). The dots are the experimental values of Haddad (Ref. 22).

In Fig. 6 the percentage difference in the transport coefficients for CH_4 calculated using two-term and converged multiterm solutions of the Boltzmann equation are shown. We see that the maximum error in the two-term approximation, for all three coefficients occurs at about 2.5—3 Td, for which $\bar{\varepsilon}\sim 0.3$ eV, and from the plot of the cross section shown in Fig. 7 it is evident that at this energy the momentum-transfer cross section is at a minimum and the inelastic processes became significant. The combined effect of this produces a large asymmetry in velocity space which makes the two-term approximation inadequate for the analysis of transport data. As the momentum-transfer cross section increases rapidly with energy beyond the minimum a decrease in the error of the two-term approximation is observed in Fig. 6 as E/n_0 increases beyond 2.5 Td. In Table III the convergence of

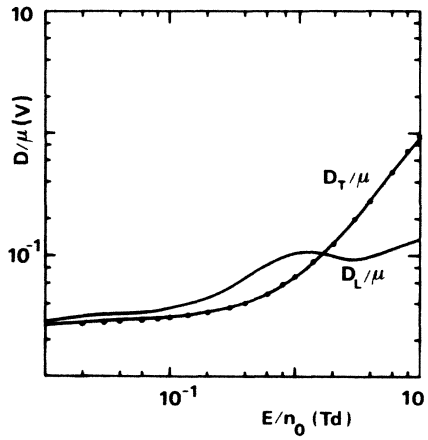

FIG. 5. The ratio of diffusion coefficients to mobility for electrons in CH_4. The dots are the experimental values of Haddad (Ref. 22).

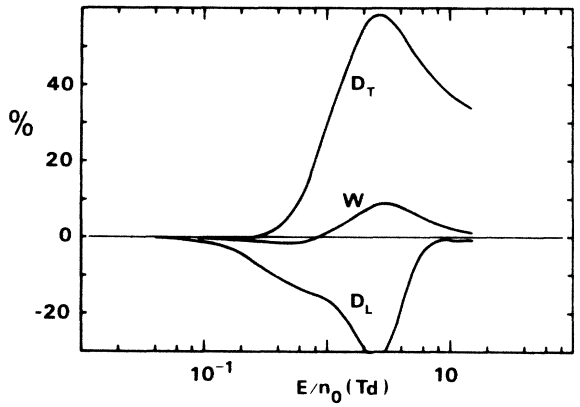

FIG. 6. Percentage difference between the two-term and multiterm solution of Boltzmann equation in the transport coefficients for electrons in CH_4.

the transport coefficients in the l index is shown for $E/n_0=3$ Td.

For $E/n_0=5$ Td the distribution functions F_0, $n_0F_0^{(L)}$, F_1, $n_0F_1^{(L)}$, $n_0F_1^{(T)}$, and $f^{(0)}(\varepsilon,\theta)$ are shown in Figs. 8, 9, and 10. The plot of $f^{(0)}$ in Fig. 10 clearly shows a large asymmetry in velocity space with $\theta=0$ being the preferred direction. This asymmetry in $f^{(0)}$ increases as ε decreases, i.e., the slower electrons have a stronger preference for $\theta=0$ motion, a reflection of the deep minimum in the elastic cross section occurring at $\varepsilon\sim 0.2$ eV.

3. *Carbon dioxide*

Electron transport in CO_2 is examined for E/n_0 in the range 0.5—50 Td. The momentum transfer and 12 inelastic cross sections of Bulos and Phelps[26] are used. Both isotropic and anisotropic[27] scattering are considered. The results of the calculation of the transport coefficients are shown in Figs. 11 and 12; also plotted in these figures are the Bulos and Phelps[26] experimental results for W and D_T/μ. As in the case of methane it appears no measurements of D_L were made. In deriving their set of cross sections, Bulos and Phelps assumed isotropic scattering and used the two-term approximation in their Boltzmann

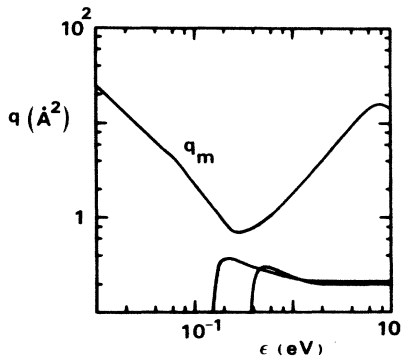

FIG. 7. Cross sections for CH_4, from Haddad (Ref. 22).

TABLE III. Convergence of the transport coefficients in the l index for electrons in CH_4, at $E/n_0=3$ Td, $T_0=293$ K.

l_{max}	W (10^5 m s^{-1})	n_0D_T (10^{24} m^{-1}s^{-1})	n_0D_L (10^{24} m^{-1}s^{-1})	D_T/μ (V)	D_L/μ (V)	$\bar{\varepsilon}$ (eV)
1	1.16	11.00±0.02	2.38	0.284	0.0617	0.383
2	1.05	5.96±0.02	3.81	0.170	0.0917	0.364
3	1.07	7.22±0.02	3.26	0.203	0.0917	0.368
4	1.07	7.01±0.02	3.37	0.197	0.0945	0.367
5	1.07	7.00±0.02	3.36	0.197	0.0944	0.367
6	1.07	7.02±0.02	3.36	0.198	0.0943	0.367
7	1.07	7.01±0.02	3.36	0.197	0.0944	0.367
8	1.07	7.01±0.02	3.36	0.197	0.0943	0.367

analysis. Comparing theory with experiment, it is evident that the coefficients obtained using isotropic scattering give the better agreement. For the low values of E/n_0 the agreement between theory and experiment is good. For the high values of E/n_0, however, disagreements up to 3% in W and 4% in D_T/μ exist. This suggests that some readjustment of the cross sections may be required, using a multiterm solution of Boltzmann's equation rather than the two-term approximation. In Fig. 13 the percentage differences between the two-term and multiterm solution for both isotropic and anisotropic scattering have been plotted. From the figure it is evident that the error in the $l=1$ approximation is significantly less for isotropic scattering when compared with that for the anisotropic scattering.

For $E/n_0=30$ Td the convergence of the transport coefficients in the l index is shown in Tables IV and V for isotropic and anisotropic scattering, respectively. Up to 22 Sonine polynomials were considered, although generally convergence was achieved by $\nu_{max}=15$. For $E/n_0=12$ Td and using the anisotropic scattering the functions F_0, $n_0F_0^{(L)}$, F_1, $n_0F_1^{(L)}$, $n_0F_1^{(T)}$, and $f^{(0)}(\varepsilon,\theta)$ were calculated, these are shown in Figs. 14, 15, and 16. Concerning the distribution functions $F_0^{(L)}$ and $F_1^{(L)}$, it is interesting to note that in all three cases plotted (Reid's model, CH_4 and CO_2) these functions change sign at $\varepsilon\sim\bar{\varepsilon}$. (This point is indicated on the energy axis by the arrow in Figs. 1, 2, 8, 9, 14, and 15.)

Using Monte Carlo techniques Braglia *et al.*[28] have obtained transport coefficients for electrons in CO_2 at $E/n_0=20$ Td, using the Bulos and Phelps cross sections, assuming isotropic scattering and setting $T_0=0$. Their results are compared in Table VI with the results of the moment solution under the same conditions. The results are in good agreement. The numbers in brackets indicate the error in the last significant figure shown and follow from the 0.5% accuracy for W and $\bar{\varepsilon}$ and 1% accuracy for D_T and D_L quoted by Braglia *et al.*[28]

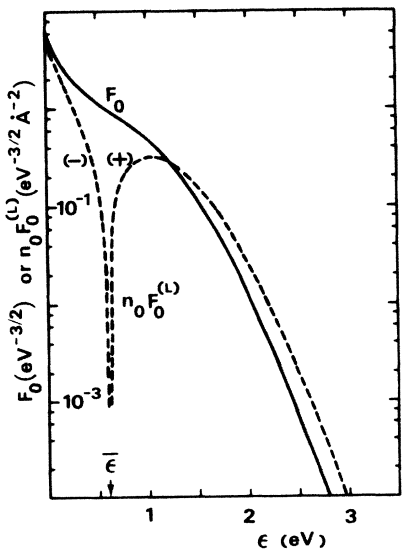

FIG. 8. Distribution functions $F_0(\varepsilon)$ and $n_0F_0^{(L)}(\varepsilon)$ for electrons in CH_4 at $E/n_0=5$ Td. Normalization as in Fig. 1.

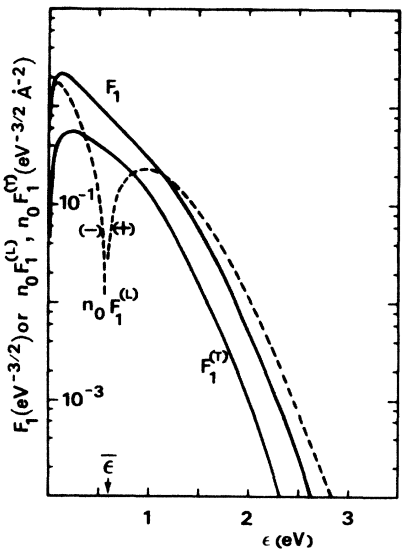

FIG. 9. Distribution functions $F_1(\varepsilon)$, $n_0F_1^{(L)}(\varepsilon)$ and $n_0F_1^{(T)}(\varepsilon)$ for electrons in CH_4 at $E/n_0=5$ Td. Normalization as in Fig. 1.

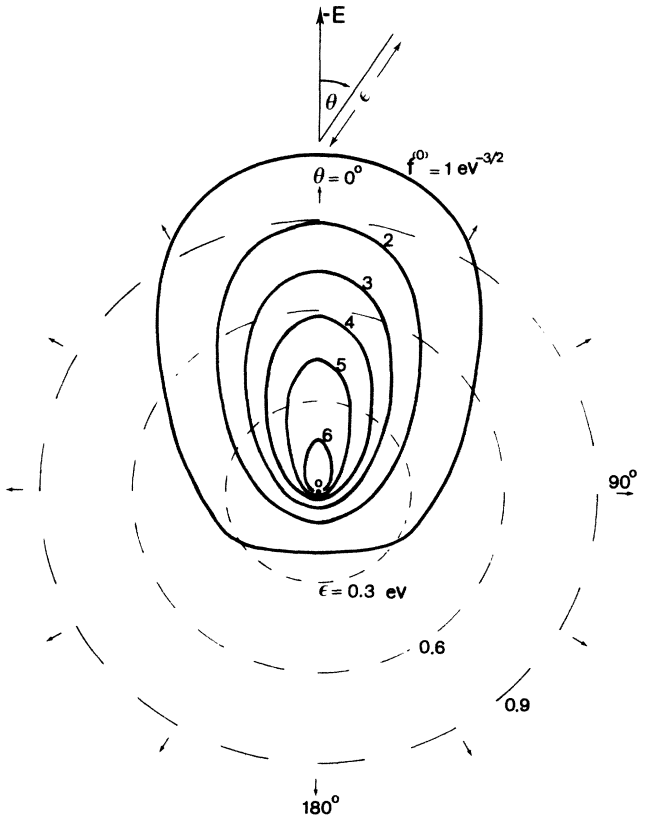

FIG. 10. Contours of constant $f^{(0)}(\varepsilon,\theta)$ for electrons in CH_4 at $E/n_0=5$ Td, $\bar{\varepsilon}=0.600$ eV. Normalization as in Fig. 3.

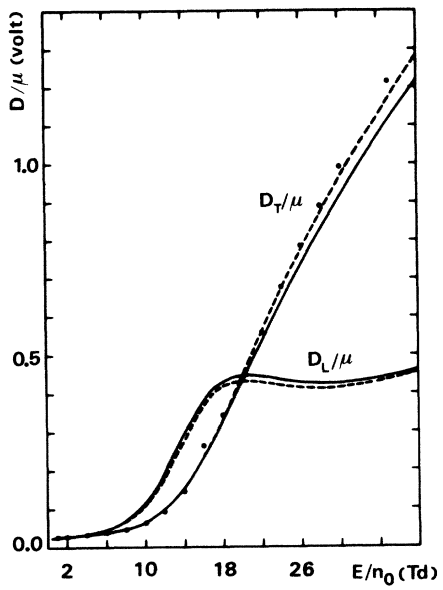

FIG. 12. Ratio of diffusion coefficients to mobility at a function of E/n_0 for electrons in CO_2, symbols, as in Fig. 11.

B. Nonconservative processes

1. Simple model calculation

To test the moment method outlined in Sec. II A for solving the Boltzmann equation when "reactions" are present, both electron attachment and ionization by electron impact are considered. To begin with, we consider the following simple model of electron attachment:

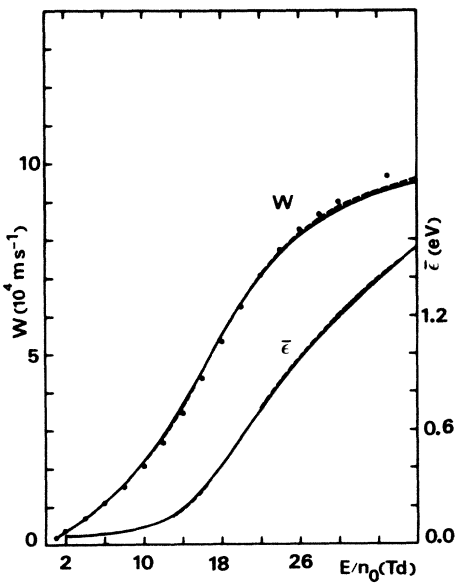

FIG. 11. Drift velocity and mean energy as functions of E/n_0 for electrons in CO_2: Anisotropic scattering (solid line), isotropic scattering (dashed line), experimental points of Bulos and Phelps (Ref. 26) (dots).

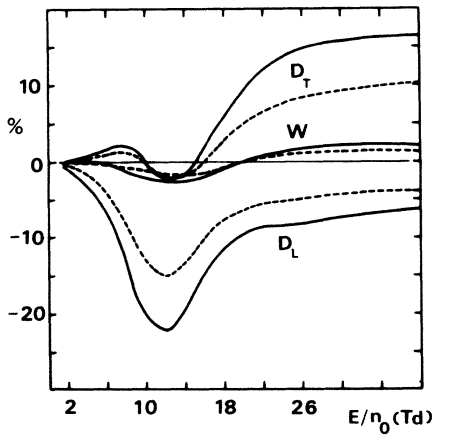

FIG. 13. Percentage difference between the two-term and multiterm solutions for transport coefficients in CO_2. Solid lines are for anisotropic scattering while the dashed lines are for isotropic scattering.

TABLE IV. Convergence of transport coefficients in the l index for electrons in CO_2: isotropic scattering, $E/n_0=30$ Td, $T_0=293$ K.

l_{max}	W (10^4 m s^{-1})	n_0D_T (10^{24} m^{-1}s^{-1})	n_0D_L (10^{24} m^{-1}s^{-1})	D_T/μ (V)	D_L/μ (V)	$\bar{\varepsilon}$ (eV)
1	8.97	3.11	1.16	1.04	0.389	1.22
2	8.85	2.84	1.22	0.964	0.414	1.21
3	8.85	2.84	1.21	0.961	0.412	1.21
4	8.86	2.85	1.22	0.964	0.412	1.21

$$\sigma_{el}=10\varepsilon^{-1/2}\ \text{Å}^2,\quad \sigma_A=a\varepsilon^p\ \text{Å}^2, \tag{54}$$

$$m_0=16\ \text{amu},\quad T_0=293\ \text{K},$$

$$\nu_A\sim\varepsilon^{p+1/2}. \tag{55}$$

For $E/n_0=0.4$ Td and $p=\frac{1}{2},-\frac{1}{2},-1$ the transport coefficients have been calculated for various values of the attachment amplitude. The results are set out in Table VII. Also shown are the quantities

$$W^*=\frac{4\pi}{3}\int_0^\infty c^3F_1(c)dc, \tag{56a}$$

$$n_0D_T^*=\frac{4\pi}{3}n_0\int_0^\infty c^3F_1^{(T)}(c)dc, \tag{56b}$$

$$n_0D_L^*=\frac{4\pi}{3}n_0\int_0^\infty c^3F_1^{(L)}(c)dc. \tag{56c}$$

That is, the quantities W^*, D_T^*, and D_L^* are W, D_T, and D_L of (I.53), respectively, excluding the *explicit* dependence upon the reactions. Note, however, that they still contain the *implicit* dependence upon reactions carried by the velocity distribution functions F_0, $F_1^{(T)}$, and $F_1^{(L)}$. In the absence of reactions $W^*\equiv W$, $D_T^*\equiv D_T$, and $D_L^*\equiv D_L$.

For all three values of p considered we see from Table VII that the attachment rate increases with a, as expected. For $p=\frac{1}{2}$ it follows from (55) that the attachment frequency increases with energy, and so the more energetic electrons are preferentially attached. This is reflected in Table VII by the decrease of $\bar{\varepsilon}$ with increasing a, i.e., attachment cooling occurs. Also note that W decreases with increasing a. As is by now well known, in the presence of the reactions the centroid velocity W has two aspects: one associated with the net transport of particles by the field and other due to a net transport brought about by the nonuniform creation or destruction of particles through the energy dependence of the reactive collision operator. Now, since the faster electrons, which tend to be at the front of the traveling swarm (as clearly indicated by the polar plots in Figs. 3, 10, and 16) are being preferentially attached, it follows that the reactions will tend to move the center of mass of the swarm in the direction opposite to the drift. Thus the centroid velocity decreases with the increasing a. The behavior of diffusion coefficients as a increase is somewhat harder to interpret. We observe that the diffusion coefficients tend to decrease as a increases, i.e., attachment cooling decreases diffusion, as it does drift. Also note that the ratio D_T/D_L, which is unity for $a=0$, increases with a, indicating that the diffusion transverse to the field increases relative to longitudinal diffusion with the increase in attachment cooling.

For $p=-\frac{1}{2}$ the attachment frequency is independent of energy, and confirming our physical expectations, we see that, apart from α/n_0, all coefficients are independent of a. There is no preferential attachment and so the reactions have no effect on the drift velocity, the diffusion coefficients, or the velocity distribution functions. Thus $W=W^*=W(a=0)$, etc.

For $p=-1$, $\nu_A\sim\varepsilon^{-1/2}$ and it follows that the slower electrons are being preferentially attached, i.e., attachment heating occurs. Thus in Table VII $\bar{\varepsilon}$ increases with a. The centroid velocity also increases with a since now the slower electrons at the back of the swarm are being removed at the faster rate, and so the reactions tend to move the center of mass in the drift direction. The coefficient D_T also increases with a, while D_L initially increases with a but then decreases for $a>5\times10^{-4}$. The ratio D_T/D_L, on the other hand, initially decreases from unity with a, but then increases for $a\geq10^{-4}$.

Concerning the quantities containing the implicit effect of the reactions only, it is observed from Table VII that W^* shows little variation with a. Only when the attachment cross section is comparable to the elastic cross section do we observe variation in W^*. This indicates that for model (54) the attachment has little effect upon the

TABLE V. Convergence of transport coefficients in the l index for electrons in CO_2: anisotropic scattering, $E/n_0=30$ Td, $T_0=293$ K.

l_{max}	W (10^4 m s^{-1})	n_0D_T (10^{24} m^{-1}s^{-1})	n_0D_L (10^{24} m^{-1}s^{-1})	D_T/μ (V)	D_L/μ (V)	$\bar{\varepsilon}$ (eV)
1	8.97	3.10	1.16	1.04	0.388	1.22
2	8.78	2.67	1.26	0.913	0.430	1.20
3	8.78	2.66	1.24	0.909	0.425	1.20
4	8.78	2.68	1.25	0.915	0.426	1.20

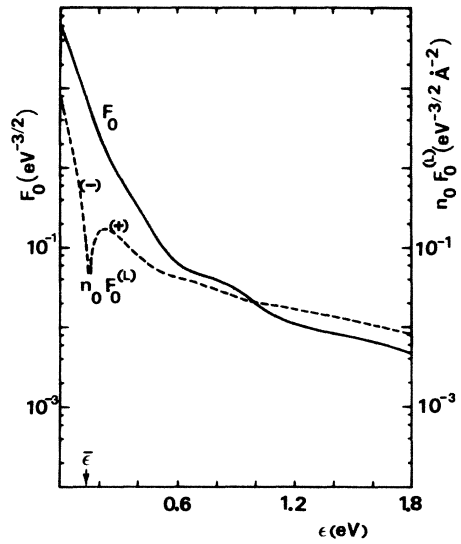

FIG. 14. Distribution functions $F_0(\varepsilon)$ and $n_0F_0^{(L)}(\varepsilon)$ for electrons in CO_2 at $E/n_0=12$ Td. Normalization as in Fig. 1.

function F_1. On the other hand D_T^* and D_L^* vary markedly with a for $p=\frac{1}{2}$ and -1, indicating that attachment has a significant effect upon the functions $F_1^{(T)}$ and $F_1^{(L)}$. The ratio D_T^*/D_L^*, however, remains unity.

For attachment cooling the electrons tend to "bunch" in the low-energy part of the distribution, and even for very large degrees of attachment ($a=10$ and beyond) the Sonine polynomial expansion converged well in calculating the transport coefficients. For attachment heating however, the electrons "bunch" in the high-energy tail of the distribution and for $a>10^{-3}$ we found a sudden deterioration in the convergence of the transport coefficients which was most pronounced for D_L. Up to 24 Sonine polynomials were considered and the indications were that many more would be required in order to obtain reliable values for all transport coefficients for $a>10^{-3}$. This implies that if the high-energy region of the actual distribution function deviates significantly from the Maxwellian, then Sonine polynomials give only a poor representation of the distribution, confirming the fact that basis sets with Maxwellian weight functions tend to place relatively little weight on the high-speed part of the function being determined.[29] In obtaining the data in Table VII, up to four terms in the l index were considered in order to check the convergence in this index, although for three-figure accuracy the $l=1$ approximation is sufficient.

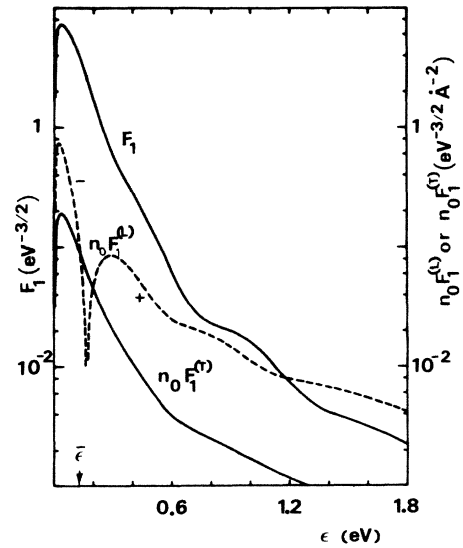

FIG. 15. Distributions functions $F_1(\varepsilon)$, $n_0F_1^{(L)}(\varepsilon)$, and $n_0F_1^{(T)}(\varepsilon)$ for electrons in CO_2 at $E/n_0=12$ Td. Normalization as in Fig. 1.

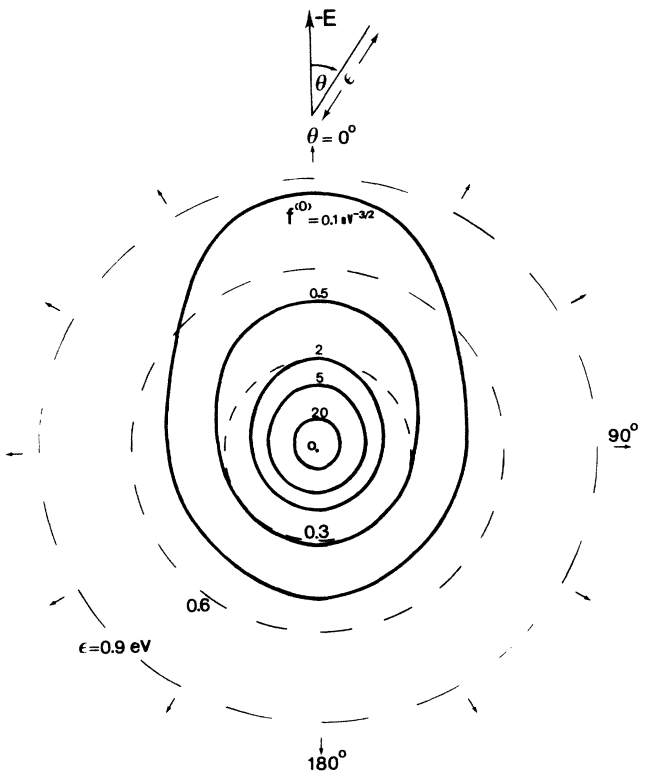

FIG. 16. Contours of constant $f^{(0)}(\varepsilon,\theta)$ for electrons in CO_2 at $E/n_0=12$ Td, $\bar{\varepsilon}=0.129$ eV. Normalization as for Fig. 3.

2. *Three-body attachment models*

The three-body attachment of electrons to neutral molecules is examined by considering model interactions. The attachment process considered is as follows:

$$M(n)+e\rightarrow M^-(*) \tag{57}$$

(the attachment collision), then

$$M^-(*)+M(n'')\rightarrow M^-+M(n''') \tag{58}$$

TABLE VI. Transport coefficients for electrons in CO_2 at $E/n_0=20$ Td. Isotropic scattering, $T_0=0$, $n_0=3.535\times10^{24}$ m^{-3}.

Code	W (10^4 m s^{-1})	D_T (10^{-1} m^{2}s^{-1})	D_L (10^{-1} m^{2}s^{-1})	$\bar{\varepsilon}$ (eV)	D_T/μ (V)
MC (Ref. 28)	6.34(3)	3.80(4)	3.89(4)	0.527(3)	0.424(6)
Moment	6.32	3.79	3.89	0.523	0.424

(the stabilizing collision), or

$$M^-(*)\rightarrow e+M(n') \tag{59}$$

(the detachment), where n is a quantum number or set of quantum numbers that denotes the internal state of the molecule M and $M^-(*)$ is an excited (unstable) state of the stable ion M^-. Once the attachment collision (57) occurs, the ion $M^-(*)$ can either undergo the stabilizing collision (58) with a third body, in this case a molecule of species M, or it can autodetach (59). In the case of (57) followed by (58) we have the attachment process

$$M(n)+e+M(n'')\rightarrow M^-+M(n''') . \tag{60}$$

In the case of (57) followed by (59) the overall process may be viewed as a conservative collision

$$M(n)+e\rightarrow e+M(n') . \tag{61}$$

Process (57) is assumed to be a resonant collision that is specified by the resonant cross section $\sigma_{res}(c)$. For low concentrations of M the rate of attachment is controlled by the stabilizing collision (58).[30] The attachment probability is then proportional to the product of the frequency ν of the stabilizing collisions and the lifetime τ of the ion state $M^-(*)$ and so we write

$$\sigma_A(c)\sim\nu\tau\sigma_{res}(c) . \tag{62}$$

Since ν is proportional to the number density n_0 of molecules M, (62) can be expressed as

$$\sigma_A(c)=Kn_0\sigma_{res}(c) , \tag{63}$$

where K is a constant, independent of n_0, that has dimensions of (length)^3. K incorporates the lifetime τ, and an efficiency factor for the stabilizing collisions (since not all stabilizing collisions may result in attachment) and is dependent upon the temperature T_0 of the molecules.

TABLE VII. Transport coefficients for model (54) at $E/n_0=0.4$ Td for $p=\frac{1}{2}$, $-\frac{1}{2}$, and -1.

a [Å^2(eV)$^{-p}$]	α/n_0 (m^{3}s^{-1})	W (10^3 m s^{-1})	n_0D_T (10^{23} m^{-1}s^{-1})	n_0D_L (10^{23} m^{-1}s^{-1})	$\bar{\varepsilon}$ (eV)	W^* (10^3 m s^{-1})	$n_0D_T^*$ (10^{23} m^{-1}s^{-1})	$n_0D_L^*$ (10^{23} m^{-1}s^{-1})
				$p=+\frac{1}{2}$				
0	0	1.186	3.055	3.055	0.1545	1.186	3.055	3.055
10^{-5}	9.153×10^{-21}	1.183	3.044	3.037	0.1543	1.186	3.051	3.051
10^{-4}	9.033×10^{-20}	1.152	2.947	2.882	0.1523	1.186	3.011	3.011
10^{-3}	8.093×10^{-19}	0.9375	2.321	1.917	0.1364	1.186	2.698	2.697
10^{-2}	5.026×10^{-18}	0.4480	1.114	0.4869	0.0847	1.186	1.675	1.675
10^{-1}	2.079×10^{-17}	0.1517	0.3984	0.08507	0.03506	1.186	0.6927	0.6928
1	7.179×10^{-17}	0.04831	0.1303	0.01853	0.01210	1.185	0.2389	0.2390
10	2.334×10^{-16}	0.01525	0.04152	0.00501	0.00393	1.183	0.0774	0.0775
				$p=-\frac{1}{2}$				
0	0	1.186	3.055	3.055	0.1545	1.186	3.055	3.055
10^{-5}	5.931×10^{-20}	1.186	3.055	3.055	0.1545	1.186	3.055	3.055
10^{-2}	5.931×10^{-17}	1.186	3.055	3.055	0.1545	1.186	3.055	3.055
1	5.931×10^{-15}	1.186	3.055	3.055	0.1545	1.186	3.055	3.055
				$p=-1$				
0	0	1.186	3.055	3.055	0.1545	1.186	3.055	3.055
10^{-6}	2.083×10^{-20}	1.190	3.066	3.069	0.1543	1.186	3.061	3.060
10^{-5}	2.060×10^{-19}	1.227	3.167	3.185	0.1572	1.186	3.107	3.107
10^{-4}	1.869×10^{-18}	1.586	4.216	4.195	0.1797	1.186	3.552	3.552
3×10^{-4}	4.783×10^{-18}	2.294	6.627	5.419	0.2219	1.186	4.386	4.386
5×10^{-4}	7.159×10^{-18}	2.898	9.054	5.656	0.2572	1.186	5.086	5.086
7×10^{-4}	9.245×10^{-18}	3.433	11.495	5.279	0.2884	1.186	5.702	5.702
9×10^{-4}	1.114×10^{-17}	3.923	13.973	4.434	0.3169	1.186	6.266	6.266
10^{-3}	1.204×10^{-17}	4.155	15.222	3.879	0.3304	1.186	6.532	6.532
2×10^{-3}	1.982×10^{-17}	6.168	28.27		0.4473	1.186	8.843	8.843
5×10^{-3}	3.76×10^{-17}	10.8	73.0		0.71	1.186	14.1	14.1

TABLE VIII. Convergence of the transport coefficients in the l index for model (75) at $E/n_0=7.5$ Td; $T_b=10000$ K, $\nu_{max}=23$, $p_0=3$ kPa, $T=9844$ K.

l_{max}	k_{att} (10^{-43} m^{6}s^{-1})	W (10^4 m s^{-1})	n_0D_T (10^{24} m^{-1}s^{-1})	n_0D_L (10^{24} m^{-1}s^{-1})
1	1.709	5.696	6.508	3.094
2	1.832	5.674	6.292	3.161
3	1.802	5.674	6.308	3.160
4	1.808	5.674	6.305	3.160
5	1.807	5.674	6.306	3.160

In terms of the space-averaged distribution function, the attachment rate is given by (I.53a), i.e.,

$$\alpha=4\pi\int J_R(F_0)c^2dc\ . \tag{64}$$

To demonstrate the pressure dependence of α, we use the Lorentz approximation for J_R, and so from (30) it follows that

$$J_R\equiv{}^AJ=n_0c\sigma_A(c)\ . \tag{65}$$

Substituting (65) into (64) gives

$$\alpha\equiv\bar{\nu}_A=n_04\pi\int F_0(c)c\sigma_Ac^2dc\ , \tag{66}$$

i.e.,

$$\alpha/n_0=4\pi\int F_0(c)c\sigma_Ac^2dc\ . \tag{67}$$

However, in view of (63) we see that in the case of three-body attachment it is the quantity

$$\alpha/n_0^2=k_{att}=K4\pi\int F_0(c)c\sigma_{res}c^2dc\ , \tag{68}$$

rather than α/n_0 that is density independent. The quantity k_{att} is known as the three-body-attachment rate coefficient.[30,31] Although the explicit density dependence has been removed from the rhs of (67), we will see later that the function $F_0(c)$ may be pressure dependent implying that k_{att} can be also pressure dependent.

From (68) it follows that

$$K=k_{att}/\langle c\sigma_{res}(c)\rangle\ , \tag{69}$$

where

$$\langle c\sigma_{res}(c)\rangle=4\pi\int F_0(c)c\sigma_{res}c^2dc\ . \tag{70}$$

For $E=0$ the electron distribution function F_0 is Maxwellian at the gas temperature if there is no preferential loss of electrons due to attachment, i.e., if $\nu_A=$const. This will otherwise only be true in the limit as $n_0\to0$, and since K is independent of n_0 we write

$$K=(k_{att})_{n_0\to0}/\langle c\sigma_{res}(c)\rangle_{n_0\to0}\ , \tag{71}$$

where $(k_{att})_{n_0\to0}$ is the three-body-attachment rate coefficient for vanishing gas density (at a given T_0) and $\langle c\sigma_{res}\rangle_{n_0\to0}$ is obtained by averaging $c\sigma_{res}$ over the Maxwellian at the gas temperature T_0. Hence given $(k_{att})_{n_0\to0}$, K and therefore σ_A can be calculated from σ_{res}. The coefficient $(k_{att})_{n_0\to0}$ can be determined by extrapolating experimental values of k_{att} back to zero density.[31]

To investigate three-body attachment the following model is used:

$$\begin{aligned}
&\sigma_{el}=3\ \text{Å}^2\ ,\\
&\sigma_{inel}=\begin{cases}0.012\ \text{Å}^2, & \varepsilon\geq0.0083\ \text{eV}\\ 0, & \varepsilon<0.0083\ \text{eV}\ ,\end{cases}\\
&\sigma_{res}=\begin{cases}0.08\ \text{Å}^2, & 0.04\leq\varepsilon\leq0.107\ \text{eV}\\ 0, & \text{otherwise}\ ,\end{cases}\\
&\sigma_A=Kn_0\sigma_{res}\ ,
\end{aligned} \tag{72}$$

with

$$K=6\times10^{-26}\ \text{m}^3,\quad m_0=32\ \text{amu},\quad T_0=296\ \text{K}\ .$$

This is a crude model of O_2 in which the inelastic cross section represents a combined average of the first 20 Gerjuoy and Stein[30,32] rotational levels and σ_{res} has been approximated from the total resonant cross section of Skullerud.[30] The value of K was chosen such that, for zero field, k_{att} for the model is of the same order as the experimental values for O_2.[31]

For model (72) the transport coefficients have been calculated for E/n_0 in the range 0—5 Td and for various gas pressures p_0. The ideal gas law

$$p_0=n_0kT_0 \tag{73}$$

is assumed. For $p_0=1$,2 and 3 kPa the coefficients α/n_0 and k_{att} are plotted in Fig. 17 as functions of E/n_0. From Fig. 17 we see that the rate coefficient α/n_0 increases with density over the entire range of E/n_0, as expected. On the other hand, the coefficient k_{att}, which is pressure dependent for low values of E/n_0, becomes pressure independent for $E/n_0>0.7$ Td. The other transport coefficients all show pressure dependence for $E/n_0<0.5$ Td. This pressure dependence of the transport coefficients arises through the pressure dependence of the attachment cross section. In the case of k_{att} the pressure dependent is due to the effect of attachment on the function $F_0(c)$. As the gas pressure increases, the attachment cross section becomes larger and the effect of electron loss in the energy region (attachment region), $0.04\leq\varepsilon\leq0.107$ eV, on the distribution function increases. As E/n_0 increases, however, the mean energy also increases (see Fig.

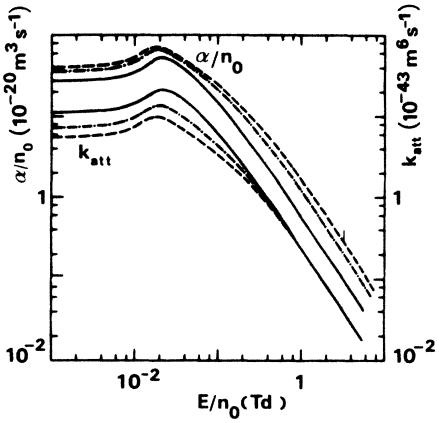

FIG. 17. Three-body attachment rate coefficient k_{att} and reaction rate coefficient α/n_0, for model (72), as functions of E/n_0 for $p_0=1$ kPa (——), $p_0=2$ kPa (—·—·—·), and $p_0=3$ kPa (— — —).

18) and as it increases above 0.107 eV (the upper threshold of attachment) there are fewer and fewer electrons available for attachment. Hence the effect of attachment on the electron distribution decreases, and for high enough E/n_0 this effect is insignificant and so k_{att} becomes pressure independent.

In the case of the other transport coefficients, W, D_T, and D_L shown in Figs. 18 and 19, the pressure dependence of the attachment cross section may affect both the implicit and the explicit dependence of these coefficients upon the reactions. However, as the attachment rate decreases with E/n_0 above 0.02 Td, the effect of attachment on both the implicit and explicit dependence decreases and, as in the case of k_{att}, for high enough E/n_0 the transport coefficients exhibit their normal hydrodynamic behavior, i.e., pressure independence.

From Figs. 18 and 19 we note that the rate of change of the transport coefficients with E/n_0 in the region 0.015—0.025 Td is rather large, and is more so for the higher pressure. This is the E/n_0 region of maximum attachment (see Fig. 17) and is also the region of change from attachment cooling to attachment heating. Consider the mean energy $\bar{\varepsilon}$ plotted in Fig. 18. For low values of E/n_0 where $\bar{\varepsilon}\sim 0.02$ eV only the high-energy electrons in the swarm can undergo attachment. Thus attachment cooling occurs, and since the higher the pressure, the greater the attachment, we observe $\bar{\varepsilon}$ to be less for the higher pressure. However, since the swarm energy increases with E/n_0, there comes a point where the lower-energy electrons of the swarm fall in the region 0.04—0.107 eV and are preferentially lost. Attachment heating then occurs and $\bar{\varepsilon}$ increases with pressure. The change over from attachment cooling to attachment heating can be pictured as occurring when the 3 kPa $\bar{\varepsilon}$ line crosses the 1 kPa $\bar{\varepsilon}$ line in Fig. 18. (The process is pressure dependent, however, and not all the different pressure lines will cross at the one E/n_0 value.)

As noted for model (54), W and D_T follow the behavior of $\bar{\varepsilon}$. Increasing p_0 for model (72) is very similar to increasing a for model (54). For attachment cooling both W and D_T decrease as the pressure (amount of attachment) increases, while for attachment heating they both increase with the pressure. [In the case of W the reason for this was explained in the preceding discussion of model (54) above.] Thus we observe in Figs. 18 and 19, respectively, the 3 and 1 kPa W and D_T lines cross once in the region of change from attachment cooling to heating. Also, as found for model (54) the behavior of D_L in the case attachment heating is more complicated. In Fig. 18, the 3 and 1 kPa D_L lines cross once in the region of change from attachment cooling to heating and then cross again in the region of attachment heating, indicating that for attachment heating D_L initially increases with the pressure, but then later decreases. This is similar to the behavior of D_L for increasing a in Table VII for $p=-1$.

As a check on our reactive moment solution, the particle-conserving moment code was applied to model (72) without the resonant cross section, and the coefficients W, $\bar{\varepsilon}$, D_T, and D_L were calculated for the higher

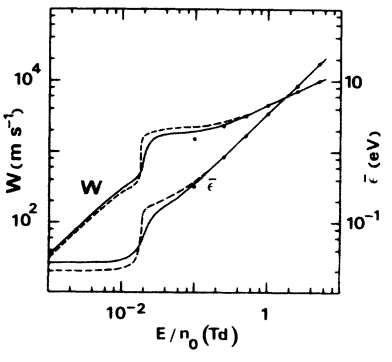

FIG. 18. Drift velocity and mean energy for model (72) as functions of E/n_0; for $p_0=1$ kPa (——) and $p_0=3$ kPa (— — —). The dots give the coefficients calculated by applying the particle conserving moment code to model (72) without the resonant cross section.

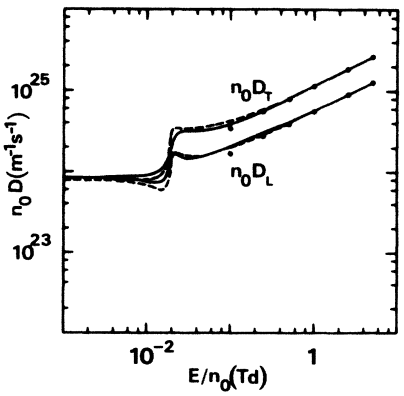

FIG. 19. Diffusion coefficients n_0D_T and n_0D_L of model (72) as functions of E/n_0 for $p_0=1$ kPa (——) and $p_0=3$ kPa (— — —). The dots have the same meaning as in Fig. 18.

values of E/n_0 where we expect the effect of the resonant attachment to be insignificant. The results are shown as dots in Figs. 18 and 19 and, as can be seen, as the attachment rate becomes insignificant the transport coefficients in the absence of reactions become identical to those in the presence of reactions.

To investigate the effect of improving the thermal contact between the electrons and neutrals on the pressure dependence of the transport coefficients, a second model is considered that is the same as model (72) except now

$$\sigma_{\text{inel}} = \begin{cases} 0.12\ \text{Å}^2, & \varepsilon \geq 0.0083\ \text{eV} \\ 0, & \varepsilon < 0.0083\ \text{eV}\ , \end{cases} \tag{74}$$

i.e., the inelastic cross section has been increased by a factor of 10. The results of transport coefficient calculations are plotted in Figs. 20 and 21. Comparing these plots with those of model (72) we observe (1) a reduction in the pressure dependence of the transport coefficients, especially for k_{att}; (2) the maximum in k_{att} and the change over from attachment heating to attachment cooling occurs at a higher value of E/n_0 ($\sim$0.05 Td compared to $\sim$0.02 Td); and (3) the behavior of the coefficients in the region of change from attachment cooling to attachment heating is less dramatic. Because of (1), gases such as N_2 and CO_2 which have good thermal contact with electrons have been added to O_2 in order to minimize the error in the measurement of the rate coefficient k_{att} in pure O_2 due to attachment cooling.[31] By increasing the thermal contact with the neutrals the electrons being lost in the attachment region (in this case 0.04—0.107 V) are more rapidly replenished and therefore the effect of attachment on the distribution function is reduced. Hence, a reduction in the pressure dependence of the transport coefficients follows. To show the effect of the improved thermal contact on the energy distribution we have plotted in Fig. 22 the energy distribution function $\varepsilon^{1/2}F_0(\varepsilon)$ at $E/n_0=0$ for models (72) and (74) and compared them with the thermal Maxwellian at 296 K.

For both models (72) and (74) considered above, accurate transport coefficients can be obtained by retaining only terms up to order $l=1$ in our polynomials expansion. To test the present theory for reactions in a situation where the two-term approximation breaks down and also to examine the pressure dependence of the transport coefficients in the presence of higher-energy inelastic processes, a third model was considered which is essentially the same as model (72) with the addition of

$$\sigma_{\text{inel}}(1) = \begin{cases} 0.1\ \text{Å}^2, & \varepsilon \geq 0.1\ \text{eV} \\ 0, & \varepsilon < 0.1\ \text{eV}\ , \end{cases}$$

$$\sigma_{\text{inel}}(2) = \begin{cases} 0.1\ \text{Å}^2, & \varepsilon \geq 0.5\ \text{eV} \\ 0, & \varepsilon < 0.5\ \text{V}\ , \end{cases} \tag{75}$$

$$\sigma_{\text{inel}}(3) = \begin{cases} 0.1\ \text{Å}^2, & \varepsilon \geq 1.0\ \text{eV} \\ 0, & \varepsilon < 1.0\ \text{eV}\ . \end{cases}$$

The higher-energy inelastic processes may be thought of as representative of vibrational or electronic excitation

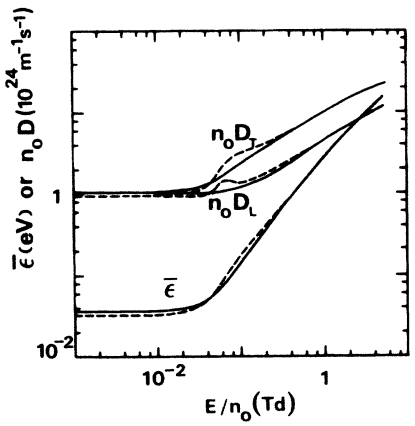

FIG. 21. Diffusion coefficients and mean energy for model (74) as functions of E/n_0 for $p_0=1$ kPa (——) and $p_0=3$ kPa (— — —).

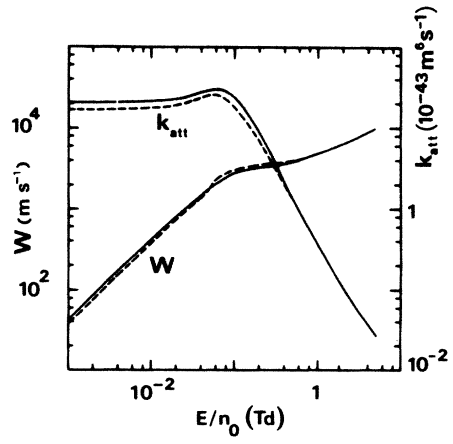

FIG. 20. Three-body attachment coefficient and drift velocity for model (74) as a function of E/n_0 for $p_0=1$ kPa (——) and $p_0=3$ kPa (— — —).

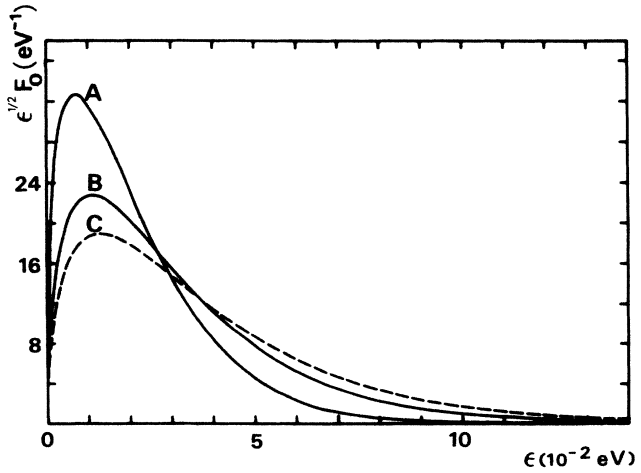

FIG. 22. Zero field energy distributions $\varepsilon^{1/2}F_0(\varepsilon)$ for models (72) (curve *A*) and (74) (curve *B*) compared with the thermal Maxwellian at 296 K (curve *C*).

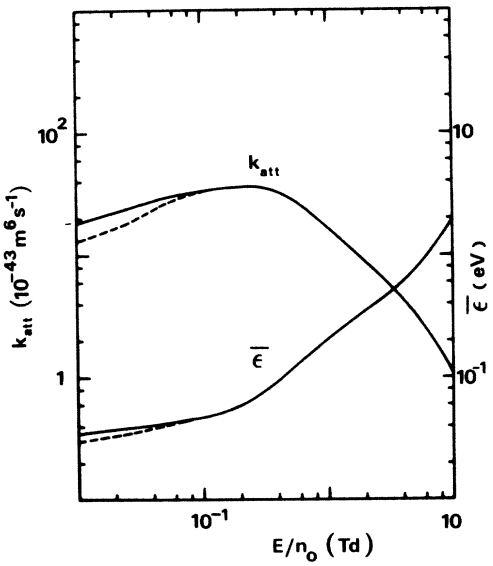

FIG. 23. Three-body attachment coefficient and mean energy for model (75) as functions of E/n_0 for $p_0=1$ kPa (——), $p_0=3$ kPa (— — —).

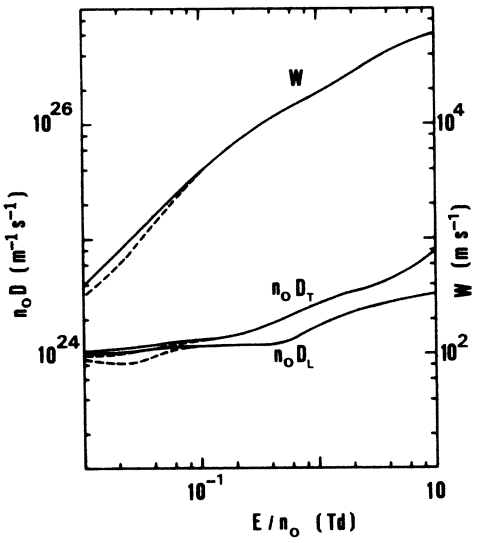

FIG. 24. Drift velocity and diffusion coefficients for model (75) as functions of E/n_0 for $p_0=1$ kPa (——) and $p_0=3$ kPa (— — —).

cross sections. Their effect is to dump the higher-energy electrons back into the low-energy region and thus we expect the resonant three-body attachment of electrons to be significant over a wider range of E/n_0 when compared to model (72). This is found to be the case, as can be seen from Fig. 23 where k_{att} and $\bar{\varepsilon}$ are plotted as functions of E/n_0 in the range 0.01—10 Td, for $p_0=1$ and 3 kPa. Comparing k_{att} in Fig. 23 with the corresponding curve in Fig. 17 for model (72) we see that for model (75) k_{att} is larger over the entire range of E/n_0, peaks at a higher value of E/n_0 (0.25 Td compared to 0.02 Td), and then decreased at a considerably slower rate with increasing E/n_0.

The other transport coefficients W, n_0D_T, and n_0D_L are shown in Fig. 24, where we see that in spite of the enhanced attachment, the transport coefficients for model (75) settle down to their usual hydrodynamic behavior at a considerably lower value of E/n_0 than the coefficients for model (72) ($\sim$0.1 Td compared to $\sim$0.7 Td). This is attributed to the large increase in thermal contact brought about by the addition of the three inelastic processes in (75). Note also from the plot of $\bar{\varepsilon}$ shown in Fig. 23 that only attachment cooling occurs, and as a consequence, the sudden changes in the transport coefficients that occurred for model (72) in the region of change from attachment cooling to heating, are no longer observed. Although for the higher values of E/n_0 there is still preferential attachment of the lower-energy electrons, these are rapidly replenished by the collisions and so no attachment heating is observed. On the other hand, for lower values of E/n_0, where the higher-energy electrons are attached, the three additional inelastic processes in (75) will not contribute significantly to the energy transfer between the electrons and neutrals, since very few electrons have sufficient energy to undergo these collisions, and so attachment cooling is still observed.

In Tables VIII and IX, the convergence of the transport coefficients in the l and ν indices are shown for model (75) at $E/n_0=7.5$ Td and in Fig. 25 the percentage difference between the two-term approximation and the converged multiterm results for the transport coefficients is plotted as a function of E/n_0. In the case of W the percentage error in the $l=1$ approximation is less than 0.5%, indicating that the two-term approximation is quite accurate for this coefficient. The accuracy in the $l=1$ approximation is not as good however, for D_L, D_T, and k_{att}.

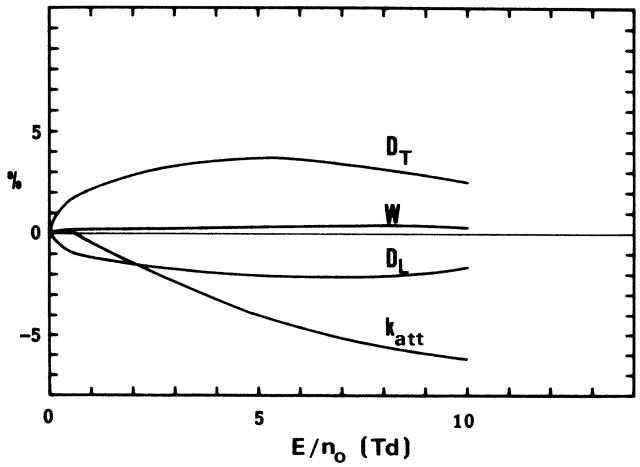

FIG. 25. Percentage difference between the two-term approximation and converged multiterm approximation in the transport coefficients for model (75).

TABLE IX. Convergence of the transport coefficients in the ν index for model (75) at $E/n_0=7.5$ Td: $T_b=10000$ K, $l_{\max}=5$, $p_0=3$ kPa.

$\nu_{\max}$	k_{att} (10^{-43} m^{6}s^{-1})	W (10^4 m s^{-1})	n_0D_T (10^{24} m^{-1}s^{-1})	n_0D_L (10^{24} m^{-1}s^{-1})
13	1.799	5.675	6.304	3.158
14	1.802	5.675	6.304	3.158
15	1.804	5.675	6.304	3.158
16	1.806	5.675	6.305	3.159
17	1.807	5.675	6.305	3.159
18	1.808	5.675	6.305	3.159
19	1.808	5.674	6.306	3.159
20	1.808	5.674	6.306	3.160
21	1.808	5.674	6.306	3.160
22	1.807	5.674	6.306	3.160
23	1.807	5.674	6.306	3.160

3. *Ionization models*

To test the theory under conditions of particle creation, the ionization model of Lucas and Saelee[33] is considered first:

$$\begin{aligned}
&\sigma_{\text{el}}=4\varepsilon^{-1/2}\ \text{Å}^2\ ,\\
&\sigma_{\text{ex}}=\begin{cases}0.1(1-F)(\varepsilon-15.6)\ \text{Å}^2, & \varepsilon\geq 15.6\ \text{eV}\\ 0, & \varepsilon<15.6\ \text{eV}\ ,\end{cases}\\
&\sigma_I=\begin{cases}0.1F(\varepsilon-15.6)\ \text{Å}^2, & \varepsilon\geq 15.6\ \text{eV}\\ 0, & \varepsilon<15.6\ \text{eV}\ ,\end{cases}\\
&P(q,\varepsilon')=1\ ,\\
&m/m_0=10^{-3},\ T_0=0\ ,\\
&n_0=10^{-20}\ \text{m}^{-3},\ E=1\ \text{Vm}^{-1},\ \text{i.e.,}\ E/n_0=10\ \text{Td}\ .
\end{aligned}\tag{76}$$

F is referred to as the degree of ionization by Lucas and Saelee,[33] who used both a Monte Carlo technique and a two-term Boltzmann solution to determine the transport coefficients for the above model. The ionization partition function[34] $[P(q,\varepsilon')]$ defines a probability density such that $P(q,\varepsilon')dq$ is the probability of one of the two electrons after ionization having a fraction between q and $q+dq$ of the available energy given that the incident electron has energy ε'. It is related to the quantity $B_0(c,c')$, defined by (40), by

$$P(q,\varepsilon')q=\tfrac{1}{2}B_0(c,c')c^3\ ,\tag{77}$$

where

$$\varepsilon'=\tfrac{1}{2}m(c')^2\ .\tag{78}$$

Setting $P(q,\varepsilon')=1$, as in the above model assumes that all the fractions $0\leq q\leq 1$ are equiprobable (AFE).

Taniguchi *et al.*[35] have also considered the above model using a two-term Boltzmann solution. The transport coefficients for model (76) have been calculated using the present theory and the results for the $l=1$ and 2 approximations are compared with those of Lucas and Saelee[33] and Taniguchi *et al.*[35] in Table X below for various values of F.

Comparing the results in Table X we see that apart from the D_L values for $F=0.5$, 0.75, and 1 the moment results and those of Taniguchi *et al.*[35] agree to within the reading error of the plots given in Ref. 35. For these D_L values, however, the moment results agree with the Boltzmann solution of Lucas. The results of Lucas, however, are rather erratic when compared with either those of the moment method or that of Taniguchi *et al.* For example, for $F=0.5$, the Boltzmann equation solution of Lucas for α and W disagrees with the other methods while Lucas's Monte Carlo results for these coefficients are in quite good agreement. On the other hand Lucas's Monte Carlo results for D_T and D_L are in disagreement, while his Boltzmann equation solution is in agreement. Similar behavior occurs for $F=1$. For both $F=0.5$ and 1 Lucas's $\bar{\varepsilon}$ results disagree with the results of the other methods. We can give no explanation for this. Only for $F=0$ (no ionization) do all four methods agree.

Taniguchi *et al.*[35] have also given values for the quantities W^* and D_T^* for model (76). In Table XI their results are compared with the present results for the $l=1$ approximation. The two methods are in good agreement.

In their work Taniguchi *et al.*[35] denote the quantities W^* and D_T^* by W_v and D_v and refer to them as the pulsed Townsend (PT) drift velocity and diffusion coefficient, respectively. Here we stress that, except when $F=0$, these are not measurable transport coefficients and although they can be calculated theoretically, we feel it is misleading to separate them from the actual transport coefficients and refer to these quantities as transport coefficients in their own right.

Finally, for model (76) we find, as did Taniguchi *et al.*,[35] that changing the ionization partitioning function to

$$P(q,\varepsilon')=\tfrac{1}{2}[\delta(1-\Delta)+\delta(\Delta)]\tag{79}$$

and setting $\Delta=\frac{1}{2}$ does not alter the transport coefficients significantly.

To investigate ionization over a range of E/n_0 values and to examine the dependence of the transport coeffi-

TABLE X. Transport coefficients for model (76): $l=1,2$ (moment method), T [Taniguchi *et al.* (Ref. 35)], L [Lucas (Ref. 33)], MC [Monte Carlo—Lucas (Ref. 33)]. Values marked with * are from Table 2(b) of Ref. 33, and values marked with † are from Table I of Ref. 35. All other values have been read from plots in Refs. 33 and 35; reading error ±0.05.

Method	α (10^3 m s^{-1})	W (10^4 m s^{-1})	D_T (10^5 m^2 s^{-1})	D_L (10^5 m^2 s^{-1})	$\bar{\varepsilon}$ (eV)
		$F=0$			
$l=1$	0	7.33	2.73	2.63	5.55
$l=2$	0	7.32	2.72	2.65	5.55
T	0	7.32†	2.74†	2.65	5.56
L	0	7.4	2.7	2.65	5.58*
MC	0	7.4	2.7	2.65	5.60*
		$F=0.25$			
$l=1$	7.14	8.03	2.75	2.72	5.37
$l=2$	7.13	8.03	2.74	2.75	5.37
T		8.0		2.8	
L		7.9		2.7	
MC		8.2		3.3	
		$F=0.5$			
$l=1$	1.34	8.59	2.76	2.76	5.21
$l=2$	1.34	8.60	2.75	2.80	5.21
T	1.3	8.6	7.75	2.9	5.23
L	1.50*	8.3	2.7	2.75	5.49*
MC	1.32	8.6	2.85	3.1	5.30*
		$F=0.75$			
$l=1$	1.91	9.06	2.77	2.78	5.07
$l=2$	1.92	9.07	2.76	2.82	5.07
T		9.1		2.9	
L		8.8		2.8	
MC		9.3		2.95	
		$F=1$			
$l=1$	2.43	9.47	2.77	2.79	4.96
$l=2$	2.43	9.48	2.76	2.84	4.96
T	2.4	9.5	2.75	2.95	4.95
L	2.93*	9.2	2.65	2.85	5.40*
MC	2.45*	9.6	2.65	2.85	5.10*

cients upon the partitioning of energy between the two electrons after ionization the following model was used:

$$\sigma_{\rm el}=10\ \text{Å}^2\ ,$$
$$\sigma_{\rm inel}=\begin{cases}1\ \text{Å}^2, & \varepsilon\geq 10\ \text{eV}\\ 0, & \varepsilon<10\ \text{eV}\ ,\end{cases}$$
$$\sigma_{\rm ion}=\begin{cases}1\ \text{Å}^2, & \varepsilon\geq 15\ \text{eV}\\ 0, & \varepsilon<15\ \text{eV}\ ,\end{cases} \tag{80}$$
$$m_0=25\ \text{amu},\quad T_0=0\ .$$

In Table XII the transport coefficients for three values of E/n_0 are shown for different choices of Δ in (79) and for $P(q,\varepsilon')=1$.

Intuitively we expect that if the transport coefficients are dependent upon how the two electrons after ionization share the available energy, then this dependence should be more apparent for the higher values of E/n_0 where the production of electrons by ionization is greater. This is observed in Table XII, i.e., as E/n_0 increases the variation of the transport coefficients with Δ increases, particularly α/n_0. The mean energy shows the least depen-

TABLE XI. The quantities W^* and D_T^* of model (76) for various values of F.

F	Method	W^* (10^4 m s^{-1})	D_T^* (10^5 m^2 s^{-1})
0	$M(l=1)$	7.33	2.73
	T	7.32	2.74
0.5	$M(l=1)$	7.34	2.57
	T	7.33	2.58
1.0	$M(l=1)$	7.34	2.44
	T	7.33	2.45

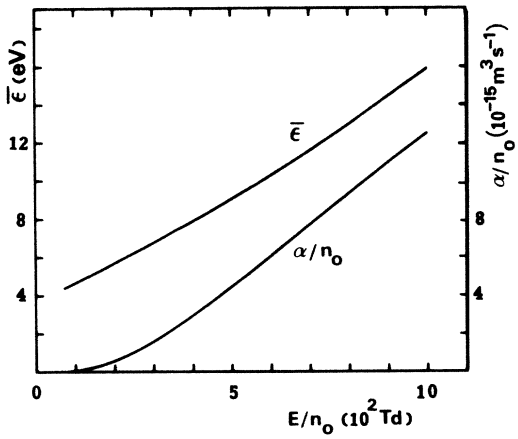

FIG. 26. Reaction rate coefficient and mean energy for model (80) with $\Delta=\frac{1}{2}$, as functions of E/n_0.

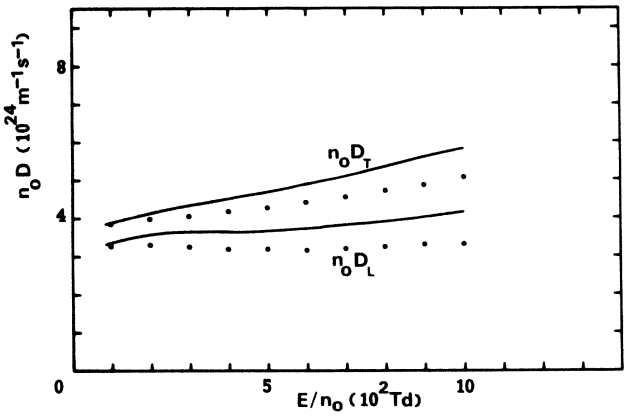

FIG. 28. Transverse and perpendicular diffusion coefficients for model (80) with $\Delta=\frac{1}{2}$, as functions of E/n_0. The dots give the quantities $n_0D_T^*$ and $n_0D_L^*$.

dence upon Δ for all values of E/n_0 considered. For $\Delta=\frac{1}{4}$, $\frac{1}{3}$, and $\frac{1}{2}$ and for AFE, W and n_0D_T also show little variation, n_0D_L and α/n_0, on the other hand, are somewhat more sensitive to the choice of these values of Δ. In the case of $\Delta=0$ all transport coefficients, apart from α/n_0 for 300 Td and $\bar{\epsilon}$ for 300 and 500 Td, show significant deviation from the values for the other choices of Δ. Setting $\Delta=0$ physically implies that after each ionization collision an electron appears at the origin of velocity space. Again, one would expect this to influence the transport coefficients for a traveling swarm, particularly as the ionization rate increases, as shown in Table XII.

The above is only a very limited investigation, since as pointed out in Ref. 4 there are many possible choices for the function $P(q,\varepsilon')$. Nevertheless, it has been sufficient to demonstrate that as the ionization rate increases it becomes increasingly more important to have an accurate knowledge of $P(q,\varepsilon')$ in order to be able to calculate the correct transport coefficients. At present it appears that $P(q,\varepsilon')$ is either set equal to 1 or to equation (79) with $\Delta=0$ or $\frac{1}{2}$. How close this is to the actual partitioning for a real gas is questionable, particularly the choice $\Delta=0$. On the basis of preliminary tests, Thomas[36] in his investigation of ionization in neon concluded that the transport coefficients were practically independent of the choice of Δ, and so set $\Delta=0$ in all his subsequent calculations. In a later investigation in neon Garamoon and Ismail,[37] in contrast to Thomas, found their results to be sensitive to the value of Δ and found $\Delta=0.5$ to give best agreement with experiment. We point out, however, that they considered only two choices of Δ, 0 and 0.5. In a subsequent investigation in argon, Ismail and Garamoon[38] set $\Delta=0.5$, while for their work on mercury vapor Garamoon and Abdelhaleem[39] considered $\Delta=0$ and 0.5 and again concluded that $\Delta=0.5$ was the better of the two. Tagashira *et al.*,[34] on the other hand, preferred to use $P(q,\varepsilon')=1$ in their analysis on argon. Brunet and Vincent[40,41] appear to have been the only ones to base their

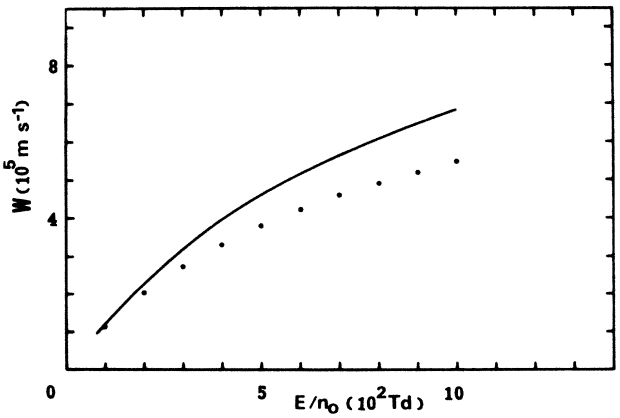

FIG. 27. Drift velocity for model (80) with $\Delta=\frac{1}{2}$, as a function of E/n_0. The dots give the quantity W^*.

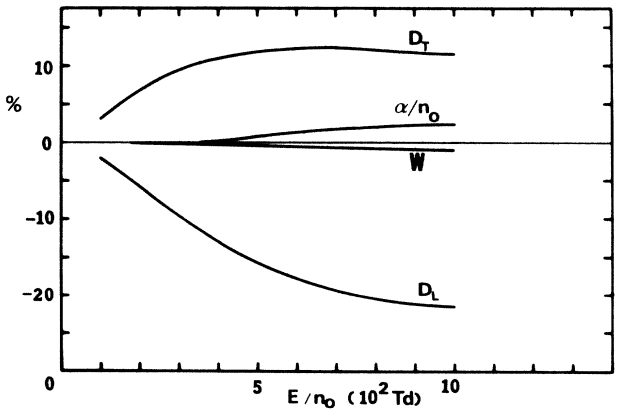

FIG. 29. Percentage difference between the $l=1$ approximation and converged multiterm approximation for the transport coefficients for model (80).

TABLE XII. Transport coefficients for model (80) at $E/n_0=300$, 500, and 800 Td for various choices of Δ and for all fractions equiprobable (AFE).

E/n_0 Td	Δ	α/n_0 (10^{-15} m^{3}s^{-1})	W (10^5 m s^{-1})	n_0D_T (10^{24} m^{-1}s^{-1})	n_0D_L (10^{24} m^{-1}s^{-1})	$\bar{\varepsilon}$ (eV)
300	0	1.61	3.23	4.29	3.79	6.73
	$\frac{1}{4}$	1.60	3.20	4.32	3.66	6.73
	$\frac{1}{3}$	1.60	3.20	4.32	3.65	6.73
	$\frac{1}{2}$	1.59	3.19	4.33	3.63	6.74
	AFE	1.51	3.19	4.32	3.68	6.75
500	0	4.68	4.74	4.61	3.95	8.99
	$\frac{1}{4}$	4.51	4.63	4.67	3.73	9.01
	$\frac{1}{3}$	4.49	4.62	4.68	3.70	9.01
	$\frac{1}{2}$	4.47	4.61	4.68	3.68	9.02
	AFE	4.37	4.62	4.68	3.77	9.04
800	0	9.62	6.25	5.28	4.25	13.21
	$\frac{1}{4}$	9.41	6.11	5.31	3.95	13.01
	$\frac{1}{3}$	9.37	6.09	5.32	3.93	12.99
	$\frac{1}{2}$	9.33	6.08	5.32	3.92	12.97
	AFE	9.20	6.12	5.34	4.01	13.09

TABLE XIII. Convergence of transport coefficients in the l index for model (80): $E/n_0=1000$ Td, $\Delta=\frac{1}{2}$, $T_b=125\,000$ K, $T=122\,878$ K, $\nu_{\max}=23$.

$l_{\max}$	α/n_0 (10^{-14} m^{3}s^{-1})	W (10^5 m s^{-1})	n_0D_T (10^{24} m^{-1}s^{-1})	n_0D_L (10^{24} m^{-1}s^{-1})	$\bar{\varepsilon}$ (eV)
1	1.279	6.748	6.453	3.256	16.03
2	1.248	6.825	5.660	4.170	15.82
3	1.249	6.817	5.830	4.145	15.90
4	1.248	6.818	5.777	4.148	15.88
5	1.249	6.818	5.794	4.146	15.88
6	1.249	6.818	5.789	4.148	15.88

TABLE XIV. Convergence of transport coefficients in the ν index for model (80). Same conditions as Table XIII; $l_{\max}=6$.

$\nu_{\max}$	α/n_0 (10^{-14} m^{3}s^{-1})	W (10^5 m s^{-1})	n_0D_T (10^{24} m^{-1}s^{-1})	n_0D_L (10^{24} m^{-1}s^{-1})	$\bar{\varepsilon}$ (eV)
13	1.251	6.820	5.780	4.141	15.86
14	1.250	6.820	5.782	4.143	15.87
15	1.250	5.819	5.784	4.144	15.87
16	1.249	5.819	5.785	4.146	15.88
17	1.246	5.819	5.788	4.147	15.88
18	1.248	6.818	5.788	4.147	15.88
19	1.248	6.818	5.788	4.148	15.88
20	1.248	6.818	5.789	4.148	15.88
21	1.248	6.818	5.189	4.148	15.88
22	1.248	6.818	5.789	4.148	15.88
23	1.249	6.818	5.789	4.148	15.88

choice of $P(q,\varepsilon')$ on experimental data in their investigations in hydrogen[40] and nitrogen.[41]

For $\Delta=\frac{1}{2}$, the transport coefficients for model (80) have been calculated for E/n_0 in the range 100–1000 Td. The results are plotted in Figs. 26, 27, and 28. In Figs. 27 and 28 the quantities W^*, D_T^*, and D_L^* have also been plotted. Comparing W with W^*, D_T with D_T^*, and D_L with D_L^* it is clear that theories[11,42] which treat ionization as just another inelastic process and ignore the generation of the new electron can at best, be valid for only small degrees of ionization. Note from Fig. 27 that ionization enhances the centroid velocity, i.e., $W>W^*$, since the ionization rate is higher for the faster electrons at the front of the swarm. We also observe in Figs. 28 that $D_T>D_T^*$ and $D_L>D_L^*$. In both Figs. 27 and 28, $W^*\to W$, $D_T^*\to D_T$, and $D_L^*\to D_L$ as E/n_0 and therefore, the ionization rates, decreases.

In Tables XIII and XIV below, the convergence of the transport coefficients in the l index and in the ν index, respectively, is shown for $E/n_0=1000$ Td.

Finally for model (80) the percentage difference between the $l=1$ approximation and the converged multiterm results for the transport coefficients have been plotted in Fig. 29. From this plot it is evident that although the two term approximation may suffice for W and α/n_0, it will fail for D_T and D_L.

IV. CONCLUDING REMARKS

In considering details of the numerical work it is important to bear in mind the fundamental role played by the interaction integrals which were mentioned in Sec. II B. These integrals must be evaluated in order to obtain the collision matrix, and from a practical point of view their accurate evaluation is essential for the subsequent successful determination of the transport coefficients. The convergence problems encountered by the original Lin-Robson-Mason code[2] in calculating the transport coefficients for some gases were traced to the failure of their Gauss-Laguerre quadrature (GLQ) to successfully evaluate the interaction integrals for certain types of cross sections varying rapidly with energy.[8] Along with other modifications, the code that calculates the collision matrix has since been altered to allow for the option of Newton-Cotes methods when GLQ is not appropriate.[8]

In general then, we have found the moment method to work well,[43] and it is particularly fast and accurate when the interaction integrals can be calculated analytically or evaluated accurately by GLQ. For the cross sections that vary rapidly with energy one must often resort to Newton-Cotes methods of integration and although accurate transport data can still be obtained, there is a marked increase in the computer time required. In such cases, however, it is believed that a significant reduction (particularly for isotropic scattering) in computer time could be achieved through the use of recurrence relationships for the interaction integrals, derived in Ref. 8.

It has been pointed out by Skullerud,[44] that moment methods cannot be expected to converge for "soft" interactions where

$$\sigma(\varepsilon)\sim\varepsilon^p,\quad p<-\tfrac{1}{2}\ .$$

For the simple elastic model of electron scattering

$$\sigma_{\rm el}=\varepsilon^{-1}\ \text{Å}^2\ ,\qquad m_0=16\ \text{amu},\quad T_0=293\ \text{K} \tag{81}$$

we have found this to be the case. Evaluating the interaction integrals exactly, we find that for $E/n_0>0.05$ Td converged values for the transport coefficients are unobtainable, although for lower values of E/n_0 the convergence is good, indicating the presence of a cutoff value in the electric field strength and possible electron runaway. Indeed, if runaway is occurring, then any hydrodynamic solution of the Boltzmann equation will break down. It is acknowledged, however, that although electron runaway is a sufficient condition for failure of the present two-temperature moment method, it is not necessary. As it was found for the attachment heating model (54) that when the high-energy region of the distribution function varied significantly from the Maxwellian form, convergence problems similar to those for model (81) for $E/n_0>0.05$ Td were encountered.

In contrast to Skullerud's comments[44] concerning the use of velocity moment methods to calculate the velocity distribution function, we find that in the case of electrons[45] these functions are obtainable. Although not as accurately calculated as the moments themselves, the accuracy is usually more than sufficient to give the form of the distribution functions over the energy range of interest for the value of E/n_0 being considered. This was demonstrated in Sec. III A 1 for Reid's inelastic ramp model by the good agreement between the present plots and those of Ref. 17.

In the situation where reactions occur two important developments were made: (1) the reactions were treated in a comprehensive and rigorous manner by going to second order in the hydrodynamic expansion and (2) a multiterm solution of the Boltzmann equation was presented. From a numerical point of view we have successfully combined a matrix inversion method with a scheme to solve the eigenvalue problem that arises when reactions occur. The success of the method has been demonstrated for the cases of electron attachment and ionization through the use of models. Examples of the attachment cooling and the attachment heating of electrons were considered and the pressure dependence of the transport coefficients due to the three-body attachment of electrons was investigated. For high ionization rates the need for more precise knowledge, concerning how the two electrons after an ionizing collision share the available energy, was shown. For low ionization rates however, this appears (from the limited investigation of Sec. III B 2) not to be too critical. The remaining step to be taken, is to apply the method to a real gas situation, e.g., the investigation of ionization in the gases considered in Refs. 34–41, as a check on the validity of the two-term approximation used by these workers. We also believe that the present moment method, with the collision matrix calculated to first order in the mass ratio, would be suitable for the study of the scattering and annihilation of slow positrons in gases.[46] The annihilation operator for positrons has the same form as the attachment operator (30) for electrons.

*Present address: Department of Chemistry, University of British Columbia, Vancouver, British Columbia, Canada Y6T 1Y6.

[1]R. E. Robson and K. F. Ness, Phys. Rev. A **33**, 2068 (1986).

[2]S. L. Lin, R. E. Robson, and E. A. Mason, J. Chem. Phys. **71**, 3483 (1979).

[3]S. Chapman and T. G. Cowling, *The Mathematical Theory of Nonuniform Gases,* 3rd ed. (Cambridge University Press, Cambridge, England, 1970).

[4]K. F. Ness, Ph.D. thesis, James Cook University of North Queensland, 1985.

[5]K. Kumar, Aust. J. Phys. **33**, 449 (1980); **33**, 469 (1980).

[6]S. L. Lin, L. A. Viehland, and E. A. Mason, Chem. Phys. **37**, 411 (1979); L. A. Viehland and S. L. Lin, *ibid.* **43**, 135 (1979).

[7]C. S. Wang-Chang, G. E. Uhleneck, and J. de Boer, in *Studies in Statistical Mechanics,* edited by J. de Boer and G. E. Uhleneck (Wiley, New York, 1964), Vol. II, p. 241.

[8]K. F. Ness and R. E. Robson, Trans. Theory Stat. Phys. **14**, 257 (1985).

[9]K. Kumar, Aust. J. Phys. **20**, 205 (1967).

[10]H. Tagashira, Proceedings of the XV International Conference on Phenomena in Ionized Gases, Minsk, USSR, 1981 (unpublished).

[11]L. G. H. Huxley and R. W. Crompton, *The Diffusion and Drift of Electrons in Gases* (Wiley, New York, 1974).

[12]We use the symbol α in this work to denote the rate of attachment of electrons to neutral molecules. Elsewhere, e.g., in Ref. 30, it is called an "attachment collision frequency" and a different symbol is used, e.g., ν_a.

[13]The first use of such terminology seems to have been by K. F. Ness, Honors thesis, James Cook University, 1977, who discussed both attachment cooling and the analogous phenomenon of diffusion cooling, plus cross effects.

[14]We continue to use α as the symbol for reaction rate, in this case, ionization production rate. Sometimes it is referred to as an "ionization collision frequency," and designated by ν_i.

[15]I. D. Reid, Aust. J. Phys. **32**, 231 (1979).

[16]L. C. Pitchford, S. V. O'Neil, and J. R. Rumble, Phys. Rev. A **23**, 294 (1981).

[17]B. M. Penetrante, J. N. Bardsley, and L. C. Pitchford, J. Phys. D **18**, 1087 (1985).

[18]D. R. A. MacMachon, Ion Diffusion Unit, Internal Rept., Australian National University, 1983 (unpublished).

[19]D. R. A. MacMahon, Aust. J. Phys. **36**, 163 (1983).

[20]P. Segur, M. Yousfi, and M. C. Bordage, J. Phys. D **17**, 2199 (1984).

[21]G. L. Braglia, L. Romano, and M. Diligenti, Phys. Rev. A **26**, 3689.

[22]G. N. Haddad, Aust. J. Phys. **38**, 677 (1985).

[23]Haddad in Ref. 22 above has also considered anisotropic scattering.

[24]R. E. Robson, Aust. J. Phys. **37**, 34 (1984).

[25]Z. Lj. Petrovic, R. W. Crompton, and G. N. Haddad, Aust. J. Phys. **37**, 23 (1984).

[26]B. R. Bulos and A. V. Phelps, Phys. Rev. A **14**, 615 (1976).

[27]The anisotropy used here is that suggested by G. N. Haddad (private communication) and is based on the work of M. A. Morrison, N. F. Lane, and L. A. Collins, Phys. Rev. A **15**, 2186 (1977); and T. W. Shyn, W. E. Sharp, and G. R. Carignan, *ibid.* **17**, 1855 (1978).

[28]G. L. Braglia, R. Bruzzese, S. Solimeno, S. Martellucci, and J. Quartieri, Lett. Nuovo Cimento **30**, 459 (1981).

[29]K. Kumar, Phys. Rep. **112**, 319 (1984).

[30]H. R. Skullerud, Aust. J. Phys. **36**, 845 (1983).

[31]R. Hegerberg and R. W. Crompton, Aust. J. Phys. **36**, 831 (1983).

[32]E. Gerjuoy and S. Stein, Phys. Rev. **98**, 1848 (1955).

[33]J. Lucas and H. T. Saelee, J. Phys. D **8**, 640 (1975).

[34]H. Tagashira, T. Sakai, and S. Sakamoto, J. Phys. D **10**, 1051 (1977).

[35]T. Taniguchi, H. Tagashira, and Y. Sakai, J. Phys. D **10**, 2301 (1977).

[36]W. R. L. Thomas, J. Phys. B **2**, 551 (1969).

[37]A. A. Garamoon and I. A. Ismail, J. Phys. D **10**, 991 (1977).

[38]I. A. Ismail and A. A. Garamoon, J. Phys. D **12E**, 1117 (1979).

[39]A. A. Garamoon and A. S. Abdelhaleen, J. Phys. D **12**, 2181 (1979).

[40]H. Brunet and P. Vincent, J. Appl. Phys. **50**, 4700 (1979).

[41]H. Brunet and P. Vincent, J. Appl. Phys. **50**, 4708 (1979).

[42]L. S. Frost and A. V. Phelps, Phys. Rev. **127**, 1621 (1962).

[43]To date only the CO_2 bench mark model [R. W. Crompton (private communication)] has presented serious problems for the moment solution. The problem was a lack of convergence in the calculation of D_L for $E/n_0=40$ Td. For $E/n_0>40$ Td, $\bar{\varepsilon}>1.8$ eV. At $\varepsilon\sim1.5$ eV there is a minimum in the elastic cross section and for $\varepsilon>4$ eV all five inelastic cross sections in the model decrease rapidly with energy. It is believed that the effect of this is to make the distribution function extremely non-Maxwellian for $E/n_0\gtrsim40$ Td, hence the lack of convergence for the moment method. Perhaps a moment solution incorporating a nonzero drift velocity parameter would be successful under such circumstances (as suggested in Ref. 4). We also note that the spline method of Pitchford *et al.* (Ref. 16) was unable to give a satsifactory D_L value [R. W. Crompton (private communication)].

[44]H. R. Skullerud, J. Phys. B **17**, 913 (1984).

[45]Skullerud in Ref. 44 restricts his comments to nonextreme mass ratios.

[46]R. I. Campeanu and J. W. Humberston, J. Phys. B **10**, 239 (1977).